Paleoceanography and Paleoclimatology

RESEARCH ARTICLE
10.1029/2020PA004179

Biotic Response to Early Eocene Warming Events: Integrated Record From Offshore Zealandia, North Tasman Sea

L. Alegret[1], D. T. Harper[2], C. Agnini[3], C. Newsam[4], T. Westerhold[5,6], M. J. Cramwinckel[7], E. Dallanave[8], G. R. Dickens[9], and R. Sutherland[10]

[1]Universidad de Zaragoza & Instituto Universitario de Ciencias Ambientales, Zaragoza, Spain, [2]Department of Geology, University of Kansas, Lawrence, KS, USA, [3]Università di Padova, Padova, Italy, [4]University College London, London, UK, [5]Now at Network Stratigraphic Consulting Ltd., Potters Bar, UK, [6]MARUM, University of Bremen, Bremen, Germany, [7]Ocean and Earth Science, National Oceanography Centre Southampton, University of Southampton, Southampton, UK, [8]Faculty of Geosciences, University of Bremen, Bremen, Germany, [9]Trinity College Dublin, Dublin, Ireland, [10]Victoria University of Wellington, Wellington, New Zealand

Key Points:

- A succession of carbon isotope excursions occurs in the early Eocene at IODP Site U1510
- Individual hyperthermal events of the Early Eocene Climatic Optimum have been identified for the first time in the Tasman Sea
- A decoupled response of benthic foraminifera and calcareous nannofossils is only observed during the largest hyperthermal

Supporting Information:

Supporting Information may be found in the online version of this article.

Correspondence to:

L. Alegret,
laia@unizar.es

Citation:

Alegret, L., Harper, D. T., Agnini, C., Newsam, C., Westerhold, T., Cramwinckel, M. J., et al. (2021). Biotic response to early Eocene warming events: Integrated record from offshore Zealandia, north Tasman Sea. *Paleoceanography and Paleoclimatology*, *36*, e2020PA004179. https://doi.org/10.1029/2020PA004179

Received 30 NOV 2020
Accepted 3 JUL 2021

© 2021. The Authors.
This is an open access article under the terms of the Creative Commons Attribution-NonCommercial-NoDerivs License, which permits use and distribution in any medium, provided the original work is properly cited, the use is non-commercial and no modifications or adaptations are made.

Abstract Environmental and biotic responses to early Eocene hyperthermal events in the southwest Pacific are critical for global paleoclimate reconstructions during Cenozoic greenhouse intervals, but detailed multidisciplinary studies are generally missing from this time and location. Eocene carbonate sediments were recovered during International Ocean Discovery Program Expedition 371 at Site U1510 on southern Lord Howe Rise in the Tasman Sea. Part of the Early Eocene Climatic Optimum (EECO; 53.26–49.14 Ma) and superimposed hyperthermal events have been identified based on refined calcareous nannofossil biostratigraphic data and carbon stable isotope records on bulk sediment and benthic foraminifera. Four negative carbon isotope excursions (CIEs) associated with negative oxygen isotope excursions are recognized within the EECO. Comparison with a global compilation of sites indicates these CIEs correlate to the K event (Eocene Thermal Maximum 3), and tentatively to the S, T, and U events. Sediments with a high carbonate content throughout the EECO provide an excellent opportunity to examine these CIEs, as carbonate dissolution often impacts correlative records elsewhere. Benthic foraminifera and calcareous nannoplankton taxa indicative of warm waters are most abundant during the K event, the most prominent hyperthermal of the EECO. Eutrophication of surface waters during the K event did not lead to increased trophic conditions at the seafloor, whereas a coupled response is observed during smaller hyperthermals. The biotic turnover sheds new light on the paleoenvironmental consequences of hyperthermal events.

1. Introduction

Progressive global warming during the early Cenozoic culminated in the Early Eocene Climatic Optimum (EECO; ca. 53.26–49.14 Ma; Westerhold et al., 2017), the warmest interval of the entire Cenozoic and the turning point toward a cooler climate during the middle and late Eocene (Barnet et al., 2019; Littler et al., 2014; Zachos et al., 2008). Sustained greenhouse warmth, as indicated by benthic foraminiferal $\delta^{18}O$ (Cramer et al., 2009; Kirtland Turner et al., 2014; Westerhold et al., 2018, 2020; Zachos et al., 2008) and biomarker-based paleothermometry (Bijl et al., 2009; Cramwinckel et al., 2018; Inglis et al., 2015), together with high atmospheric CO_2 concentrations (e.g., Anagnostou et al., 2016; Beerling & Royer, 2011), potentially due to increased volcanic emissions (Pearson & Palmer, 2000; Royer et al., 2007), indicate that greenhouse gas levels and both sea surface (Inglis et al., 2020) and deep-sea temperatures were considerably higher than present. These features make the EECO a significant ancient archive to test and improve models that predict our future climate (Hollis et al., 2019).

The long-term climate changes of the early and middle Eocene were punctuated by a series of rapid warming events associated with negative carbon and oxygen isotope excursions (CIEs, OIEs) in bulk marine carbonate and benthic foraminiferal stable isotope records. These "hyperthermals" were somehow linked to massive releases of ^{13}C depleted carbon into the ocean-atmosphere system (see discussion in Dickens, 2011), and their continuity in magnitude and frequency reflects orbital forcing of the carbon cycle (Kirtland Turner et al., 2014; Lourens et al., 2005; Lunt et al., 2011; Zeebe & Lourens, 2019). Two large, well-defined

Printed by [Icelandair ehf - 185.056.012.142 - /doi/epdf/10.1029/2020PA004179] at [04/08/2021].

hyperthermals follow the largest one, the Paleocene-Eocene Thermal Maximum (PETM; ~56 Ma); these are superimposed on the overall warming trend toward the EECO, and referred to as Eocene Thermal Maximum 2 (ETM2, ~53.7 Ma, also known as Elmo or the H1-event; Lourens et al., 2005) and Eocene Thermal Maximum 3 (ETM3, ~52.4 Ma, also known as the K- or X-event; Cramer et al., 2003; Röhl et al., 2005). After ambiguous definition for the duration of the EECO (e.g., Lauretano et al., 2015; Luciani et al., 2016; Westerhold & Röhl, 2009; Zachos et al., 2008), its onset is now placed between these two events, at the J event (C24n.2rH1, 53.26 Ma; Thomas et al., 2018). The J event is marked by a negative CIE and OIE in the Atlantic Ocean (D'Onofrio et al., 2020; Lauretano et al., 2015), and coincides with a major lithological change in pelagic carbonate sequences in New Zealand (Hollis et al., 2005), perhaps related to hydrological change (Dallanave et al., 2015; Slotnick et al., 2012, 2015). With a termination assigned to Chron C22n CIE, C22nH5 (49.14 Ma) (Hollis et al., 2019; Westerhold et al., 2017), the EECO spans 4.12 Myrs and includes several hyperthermal events.

ETM3, here referred to as the K event following the nomenclature in Westerhold et al. (2017), stands out as a prominent hyperthermal in records from widespread locations, including Atlantic drill sites (Cramer et al., 2003; D'Onofrio et al., 2020; Luciani et al., 2017; Röhl et al., 2005; Thomas et al., 2018), uplifted Tethys Ocean sections (Agnini et al., 2009; Galeotti et al., 2019), equatorial Pacific drill sites (Bhattacharya & Dickens, 2020; Bralower, Parrow, et al., 1995; Bralower, Zachos, et al., 1995; Cramer et al., 2003; Westerhold et al., 2018), and uplifted southwest Pacific sections in New Zealand (Slotnick et al., 2012, 2015). In bulk carbonate stable isotope records, $\delta^{13}C$ and $\delta^{18}O$ values typically drop rapidly by about 0.6‰ followed by a logarithmic recovery.

Analyzing the biotic response to past warm intervals such as the EECO and the K event may clarify consequences of future climate change. The biotic consequences of the PETM have been documented from a global distribution of sites, and include poleward migration of terrestrial and marine taxa and the largest Mesozoic-Cenozoic deep-sea benthic foraminiferal extinction (e.g., Alegret et al., 2021; Alegret, Ortiz, Orue-Etxebarria, et al., 2009; Alegret, Ortiz & Molina, 2009; Speijer et al., 2012; Thomas, 2007). Comparison of the biological changes at the PETM with changes during hyperthermals of reduced magnitude may aid our understanding of how biotic response scales with warming, but studies concerning the biotic consequences of smaller hyperthermals are much more limited (see references in Thomas et al., 2018), in particular those dealing with the K event. In the Pacific realm, the benthic foraminiferal turnover across the K event has been documented only at equatorial Pacific Ocean Drilling Program (ODP) Site 865 (Leg 143; Arreguín-Rodríguez et al., 2016). To date, only two studies have correlated biotic changes in the deep sea (benthic foraminifera) to those in the surface waters (calcareous nannofossils or planktic foraminifera) to provide an integrated water column perspective across the K event: a high-resolution record in the South Atlantic (Walvis Ridge IODP Sites 1262 and 1267; Thomas et al., 2018) and an integrated study from the Tethys Ocean (Farra section; Agnini et al., 2009).

Early Eocene records of the southwest Pacific are of particular interest in terms of climate dynamics because of their proximity to a major source of deep water in the Southern Ocean sector (Huck et al., 2017) at a time when the Pacific Ocean was the primary driver of ocean heat transport (Huber & Nof, 2006). Peak EECO warmth (as inferred from sea surface temperature proxies) at the mid-Waipara River section (New Zealand) coincides with an increase in warm-water calcareous nannofossil and dinocyst taxa, and a high abundance of planktic foraminifera (Crouch et al., 2020; Hollis et al., 2009, 2012). However, detailed quantitative paleontological records across the K event have not been described. Previous ocean drilling expeditions (DSDP Legs 21, 29, 90, and 91) in the Tasman Sea (southwestern Pacific) were aimed at reconstructing the paleoceanography and the tectonic history of this region, but early Eocene carbonate-bearing sediments were only obtained from a few sites (Sites 206, 207, and 210; Shipboard Scientific Party, 1973a, 1973b, 1973c), with poor recovery across the EECO. The early to middle Eocene was recovered on the western margin of the Campbell Plateau (DSDP Site 277; Shipboard Scientific Party, 1975), but low-resolution geochemical studies (Shackleton & Kennett, 1975) did not allow identification of individual hyperthermal events within the EECO. The EECO is also recorded in marginal marine sediments of the East Tasman Plateau (ODP Leg 189, Site 1172; Bijl et al., 2009), but calcareous fossils are virtually absent. TEX_{86}-based sea surface temperatures (SSTs) from both this site and mid-Waipara indicate near-tropical conditions (between 24°C and 31°C)

Printed by [Icelandair ehf - 185.056.012.142 - /doi/epdf/10.1029/2020PA004179] at [04/08/2021].

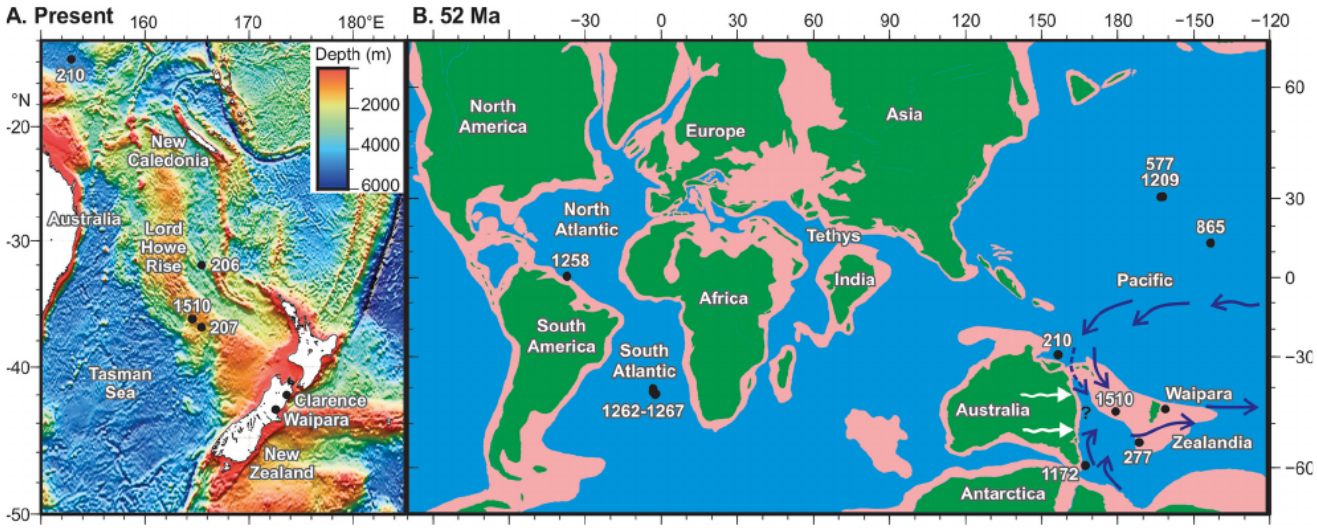

Figure 1. Location of the study site. (a) Present day location of Site U1510 and other sites mentioned in the text in the Tasman Sea area. (b) Global paleogeographic reconstruction at 52 Ma in a paleomagnetic reference frame (after Cook et al., 1999; Matthews et al., 2016; Sutherland et al., 2020; Torsvik et al., 2012). Green areas are regions inferred to be land, and pink is shelf to lower bathyal environments (Cao et al., 2017). The blue arrows show approximate locations of ocean currents near Site U1510 (after Hollis et al., 2012).

during the EECO, followed by 2°C–4°C cooling during the early middle Eocene transition, starting at ca. 49 Ma (Bijl et al., 2013).

Reconstructions of biogeographic patterns of surface-dwelling plankton can be used to infer past surface-ocean circulation, and indicate that early Eocene conditions in the Tasman Sea were characterized by gyral circulation without significant throughflow through the Tasmanian Gateway (Bijl et al., 2013; Huber et al., 2004). Increased southward expansion of a warm proto-East Australian Current has been suggested to explain peak warmth in the early (Hines et al., 2017; Hollis et al., 2012) and middle (Cramwinckel et al., 2020) Eocene. Shallow westward surface circulation through the Tasmanian Gateway of a proto-Antarctic Counter Current likely started near the end of the EECO, from ~50 Ma onwards (Bijl et al., 2013; Sijp et al., 2016).

Here, we present a multidisciplinary high-resolution analysis of carbonate-bearing, early Eocene sediments in the north Tasman Sea that complements previous studies to the south and on mainland New Zealand. We use early Eocene sediments recovered during International Ocean Discovery Program (IODP) Expedition 371 at Site U1510 to generate micropaleontological data on benthic foraminifera and calcareous nannofossils as proxies for conditions at the seafloor and in surface waters, respectively. Combined with geochemical analyses (carbon and oxygen stable isotopes on bulk sediment and benthic foraminifera) and a refined age model, we infer the biotic and paleoenvironmental consequences of hyperthermal events across a critical time of Earth's history in the Tasman Sea. A new age model was implemented to compare and correlate this record with a global compilation of sites, shedding new light on the consequences of the warmest period of the Cenozoic.

2. Materials and Methods

IODP Site U1510 (36°19.74′S, 164°33.52′E; 1238 m water depth) is located on southern Lord Howe Rise, ~850 km west of northern New Zealand (Sutherland et al., 2018, Sutherland, Dickens, Blum, Agnini, Alegret, Asatryan, et al., 2019, Sutherland, Dickens, Blum, Agnini, Alegret, Bhattacharya, et al., 2019; Figure 1). A 480 m thick sequence of Pleistocene to lower Eocene nannofossil ooze and chalk was recovered (Sutherland, Dickens, Blum, Agnini, Alegret, Bhattacharya, et al., 2019). During the early Eocene, this site was located at a middle bathyal setting on a ridge (Sutherland et al., 2020) that may have underlain the boundary zone between the warm subtropical proto-East Australian Current and the cold subantarctic Tasman Current (Figure 1), somewhat analogous to the present-day subtropical front. Here we analyze

Printed by [Icelandair ehf - 185.056.012.142 - /doi/epdf/10.1029/2020PA004179] at [04/08/2021].

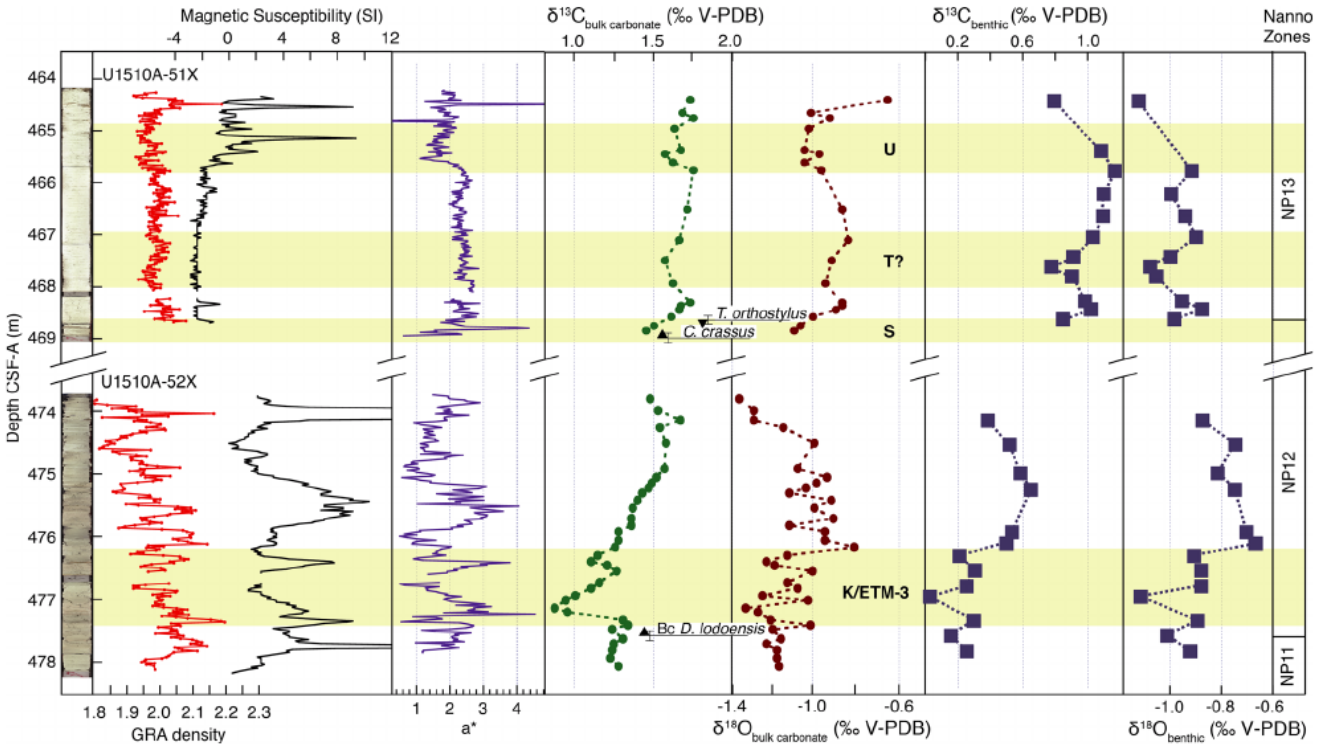

Figure 2. Physical properties (Sutherland, Dickens, Blum, Agnini, Alegret, Bhattacharya, et al., 2019), carbon and oxygen stable isotopes on bulk sediment and benthic foraminifera (*N. truempyi*), and calcareous nannofossil biozones from Cores U1510A-51X and 52X, plotted against depth.

Cores U1510-51X and 52X comprising lower Eocene planktic foraminiferal zones E4 to E7 and calcareous nannofossil zones NP11, NP12, and NP13 (Martini, 1971), or CNE3, CNE4, and CNE5 (Agnini et al., 2014). Sediments of Core U1510-51X are white nannofossil chalk with small cm-size, relatively light colored chert nodules in section CC. The core is severely biscuited throughout, and the slurry between the biscuits was carefully avoided during sampling. Core U1510-52X consists of nannofossil chalk with a slight change in sediment color from white to light greenish gray and pinkish white that coincides with a downhole decrease in the sedimentation rate and increase in magnetic susceptibility. Coring disturbance of both Cores U1510-51X and -52X, combined with the very low magnetic remanence, hampered a reliable magnetic polarity age control (Sutherland, Dickens, Blum, Agnini, Alegret, Bhattacharya, et al., 2019).

Shipboard nannofossil biostratigraphy and physical property data (i.e., red over green ratio of lightness (a* ratio), magnetic susceptibility (MS), and GRA density; Figure 2) were used to guide bulk carbonate stable isotope sampling, targeting the early Eocene interval in Cores U1510A-51X and -52X (Data Set S1). A total of 54 samples were selected at ~10–20 cm intervals, dried for 12 h at 50 °C in a vacuum oven, and homogenized with a mortar and pestle. Approximately 60 μg of homogenized material was then sampled for $\delta^{13}C$ and $\delta^{18}O$ analysis via Isotope Ratio Mass Spectrometry (IRMS) using a Thermo Fisher Scientific MAT 253 with a Kiel IV carbonate device at the University of California, Santa Cruz. Long-term reproducibility in standards (e.g., Carrara Marble) indicates precision for $\delta^{13}C$ and $\delta^{18}O$ (1σ) of ±0.05‰ and ±0.08‰, respectively.

A total of 40 samples were processed for benthic foraminiferal studies. Samples were oven-dried at 40°C, weighed to obtain bulk dry sample weight, and soaked and disaggregated in a cold sodium hexametaphosphate ($Na_6[PO_3]_6$) solution, then washed with tap water over a 63 μm wire mesh sieve. The residue was oven-dried at 40°C and weighed. Benthic foraminifera test carbonate was measured for $\delta^{13}C$ and $\delta^{18}O$ on 40 samples at MARUM stable isotope facilities. Each measurement was made using a single species (the epifaunal *Nuttallides truempyi*, or the infaunal *Oridorsalis umbonatus* and *Aragonia aragonensis*) (Data Set S1; Figure S1). Analyses at MARUM were performed on ThermoFisher Scientific 253plus gas isotope ratio mass spectrometer with Kiel IV automated carbonate preparation device. Samples were reacted with

Printed by [Icelandair ehf - 185.056.012.142 - /doi/epdf/10.1029/2020PA004179] at [04/08/2021].

orthophosphoric acid at 75°C. Analytical precision based on replicate analyses of in-house standard (Solnhofener Limestone) averages 0.03‰ and 0.04‰–0.06‰ (1σ) for $\delta^{13}C$ and $\delta^{18}O$, respectively. Data are reported relative to the Vienna Pee Dee Belemnite international standard, determined via adjustment to calibrated in-house standards and NBS-19.

Quantitative studies of benthic foraminifera larger than 63 μm were performed on a subset of 28 samples, and based on representative splits of approximately 280–300 specimens (Data Set S2). Diversity of the assemblages (Fisher-α index; Murray, 2006), the calcareous to agglutinated benthic foraminiferal ratio and the relative abundance of the Superfamily Buliminacea (following Sen Gupta, 1999) were calculated (Data Set S2). Taxa were allocated into infaunal and epifaunal morphogroups to infer oxygenation and trophic conditions in the deep ocean, with epifaunal morphogroups generally more abundant in oligotrophic environments (Jorissen et al., 2007). Caution must be taken with a simplistic interpretation of morphogroups, however, as it is problematic even for living foraminifera (Buzas et al., 1993) and the lack of modern analogs makes it less straightforward for fossil assemblages (Hayward et al., 2012), especially when significant changes in relative abundance of species of the same morphogroup result in a constant total abundance of that morphogroup (e.g., Alegret & Thomas, 2009; Alegret et al., 2021). The benthic foraminiferal accumulation rates (BFAR), a proxy for delivery of organic matter to the seafloor (Jorissen et al., 2007), were calculated following Herguera and Berger (1991) using the number of benthic foraminifera per gram of sediment >63 μm, the weight % of the sample >63 μm, the sediment density (Sutherland, Dickens, Blum, Agnini, Alegret, Bhattacharya, et al., 2019), and the linear sedimentation rates as obtained from the refined age model (Figure S2). BFAR values, however, are strongly determined by the number of foraminifera per gram ($r^2 = 0.9$; Figure S3 and Data Set S2), and the lack of sedimentation rate information at the required time resolution does not allow to infer whether changes in BFAR across hyperthermal events indicate changes in productivity of foraminifera, or in sedimentation rates. Consequently, interpretations on the trophic conditions at the seafloor are based on the relative abundance of benthic foraminiferal taxa. Detrended Correspondence Analysis (DCA) and hierarchical cluster analysis in Q-mode (samples) contributed to paleoenvironmental interpretations. Statistical analyses of a reduced data set of 26 species of benthic foraminifera were made with PAST software (Hammer et al., 2001), using the unweighted pair-group average algorithm (UPGMA), and the Pearson correlation as similarity coefficient.

To improve shipboard calcareous nannofossil biostratigraphy (Sutherland, Dickens, Blum, Agnini, Alegret, Bhattacharya, et al., 2019) and to investigate the response of calcareous nannofossils, 64 samples were analyzed. These include the 40 samples analyzed for benthic foraminifera studies, plus 24 additional samples. Standard and additional biohorizons were identified and/or refined to improve the shipboard age model by using semiquantitative counts (N/mm^2, Backman & Shackleton, 1983). Quantitative analyses of at least 300 forms were performed to monitor assemblage fluctuations and provide paleoecological and paleoenvironmental interpretations. Calcareous nannofossils were examined on standard smear slides (Bown & Young, 1998) and were analyzed using standard light microscope techniques under crossed polarizers, transmitted light, and phase contrast at 1000X or 1250X magnification on a Zeiss Axiophot microscope. The biozonations applied in this work are those of Martini (1971) and Agnini et al. (2014), and the stratigraphic positions and age of biohorizons are summarized in Table S1. We followed the taxonomy of Aubry (1984, 1988, 1989, 1990, 1999), Perch-Nielsen (1985) and Bown (2005), and the relative and semi-quantitative abundance of identified taxa are included in Data Sets S3 and S4, respectively.

A set of seven evenly spaced samples over Core U1510A-52X and one sample from the base of Core -51X were assessed for the potential for organic geochemical analyses. Lipids were extracted using a Dionex accelerated solvent extractor (ASE 350), followed by Al_2O_3 column chromatography and analysis of the polar lipid fraction using high-performance liquid chromatography-mass spectrometry (HPLC-MS) at Utrecht University. Unfortunately, concentrations of GDGTs were approximately an order of magnitude too low for reliable TEX_{86} paleothermometry.

Additionally, the weight %$CaCO_3$ was analyzed at Zaragoza University, and the coarse fraction was calculated as the weight ratio of the dry ≥63 μm size fraction to the bulk dry sediment weight (Data Set S2). The drilling rate of penetration (ROP) was calculated from operational data recorded by the Rig Watch drilling information system on RV *JOIDES* Resolution (Data Set S5). Weather conditions were challenging (marginal) during drilling, with 3–5 m swell. Wave noise was suppressed by median filtering the block position

Printed by [Icelandair ehf - 185.056.012.142 - /doi/epdf/10.1029/2020PA004179] at [04/08/2021].

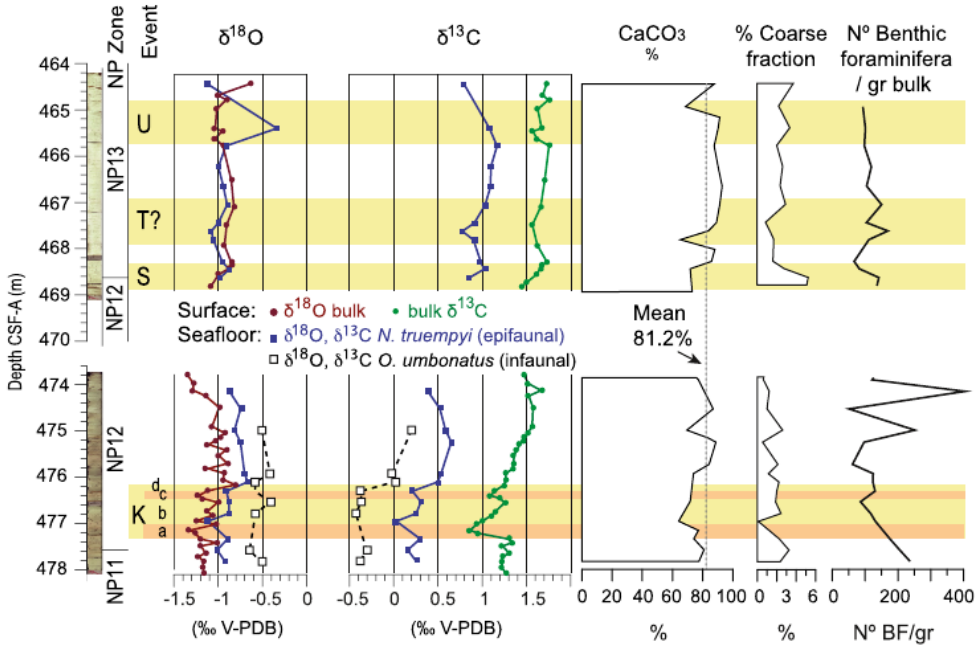

Figure 3. Stable isotopes, % $CaCO_3$, relative abundance of coarse fraction (CF) and number of benthic foraminifera per gram at Site U1510, plotted against depth.

over a 5 min sliding window. ROP values were then resampled onto a regular 5 cm depth mesh and median filtered over a 30 cm sliding window.

3. Identification of Events

3.1. Stable Isotopes and Physical Properties

Bulk carbonate $\delta^{13}C$ ranges from 0.6‰ to 1.8‰ in Cores U1510A-51X and -52X, exhibiting variability characteristic of early Eocene carbon isotope excursions (negative CIEs; Figure 2). Bulk carbonate $\delta^{18}O$ ranges from −1.1‰ to −0.6‰ with variability coincident with shifts in $\delta^{13}C$. Both $\delta^{13}C$ and $\delta^{18}O$ steadily increase up-section, and background bulk $\delta^{18}O$ is lighter in Core U1510A-51X compared to Core U1510A-52X. Core U1510A-52X contains the largest CIE in our study record: $\delta^{13}C$ decreases by 0.4‰ starting at ~477.21 m CSF-A and nearly recovers to baseline values prior to a second smaller $\delta^{13}C$ decrease of ~0.2‰ at ~476.46 m CSF-A. $\delta^{13}C$ fully recovers to pre-excursion values by ~476.17 m CSF-A. Negative oxygen isotope excursions (OIEs) in bulk carbonate of 0.3‰ and 0.2‰ are associated with the 0.4‰ and 0.2‰ CIEs, respectively. Bulk carbonate $\delta^{13}C$ and $\delta^{18}O$ increase by a respective 0.3‰ and 0.2‰ from the base of Core U1510A-51X (sample depth of 468.80 m CSF-A) up to 468.33 m CSF-A. Two additional stable isotope excursions (i.e., 0.1‰–0.2‰ decreases in both $\delta^{13}C$ and $\delta^{18}O$) are recorded in the upper 4 meters of Core U1510A-51X (Figure 2).

Mono-specific $\delta^{13}C$ analyses of benthic foraminifera range from 0.03‰ to 1.17‰ for the epifaunal species *N. truempyi* (Figure 2) and from −0.4‰ to +0.2‰ for the infaunal *O. umbonatus* (Figure 3), and show an overall increasing trend up-section interrupted by negative CIEs. The largest one is recorded in Core U1510A-52X, marked by a ~0.3‰ decrease in *N. truempyi* (and ~0.15‰ in *O. umbonatus*) coeval with the main drop in bulk carbonate $\delta^{13}C$, and followed by recovery to baseline values prior to a second smaller $\delta^{13}C$ decrease of ~0.1‰ in *N. truempyi* at ~476.46 m CSF-A. These excursions are associated with negative OIEs in *N. truempyi* of 0.2‰ and 0.1‰, respectively. Benthic $\delta^{13}C$ values above the double excursion in Core U1510A-52X are more positive than pre-excursion values. The baseline positive shift in bulk $\delta^{18}O$ and benthic $\delta^{13}C$ and $\delta^{18}O$ at ~476.20 m CSF-A likely indicates a small unconformity whose duration falls outside the detection limits of calcareous nannofossil biozones. Since the double-trough $\delta^{13}C$ excursion characteristic of the K event is well recorded at Site U1510, it follows that the unconformity at its top did not affect the event, but its aftermath.

Printed by [Icelandair ehf - 185.056.012.142 - /doi/epdf/10.1029/2020PA004179] at [04/08/2021].

The only two benthic $\delta^{13}C$ and $\delta^{18}O$ data-points at the base of Core U1510A-51X parallel the increase in bulk carbonate $\delta^{13}C$ and $\delta^{18}O$ values up to 468.33 m CSF-A. Benthic $\delta^{13}C$ and $\delta^{18}O$ values record an additional negative excursion (−0.20‰ and −0.12‰, respectively) at ~467.94 m CSF-A.

The typical surface-to-deep $\delta^{13}C$ gradient is observed in Core U1510A-52X (Figure 3), and infaunal benthic $\delta^{13}C$ values (*O. umbonatus*) are also lighter than epifaunal ones (*N. truempyi*), as expected (e.g., Schmiedl et al., 2004). The vertical $\delta^{13}C$ gradient is slightly reduced in Core U1510A-51X. The surface-to-deep $\delta^{18}O$ gradient is very weak and it even reverses in Core U1510A-51X (Figure 3), suggesting that the $\delta^{18}O$ record may have been affected by diagenesis and carbonate dissolution and reprecipitation after deposition on the seafloor. A similar mechanism accounts for the reduced planktic-to-benthic temperature gradient during the middle Eocene at Site 277, as compared to the mid-Waipara section (Hollis et al., 2009). Both locations and Site U1510 correspond to middle to lower bathyal paleodepths.

The mean $CaCO_3$ content is 81.2%, and values range from 92.9% to a minimum of 64.1%. The three lowermost values at 476.96, 467.8, and 464.92 m CSF-A fall within intervals of decreased $\delta^{13}C$ values (Figure 3; Data Set S2). Physical property records measured on the surface of the split cores, particularly a* ratio and MS (Figure 2), can help characterize hyperthermal events in deep sea records (Lourens et al., 2005). The terrigenous sediment fraction typically increases during these transient events due to carbonate dissolution, enhanced siliciclastic dilution or both. Carbonate-rich sediments have low a* ratios and MS, but these increase with elevated terrigenous content because this material tends to give the sediment a reddish-brown color and contains magnetic components. In core U1510A-52X, the lowermost $\delta^{13}C$ values coincide with higher a* ratios and positive peaks in MS. In core U1510A-51X, this relationship is less clear but at least at the top and bottom of the core, higher values of a* ratio and MS coincide with more depleted $\delta^{13}C$ data. GRA density data from both cores are disrupted by drilling-induced disturbance of the sediment, typical for XCB drill cores. For this reason, discrete shipboard sample dry bulk density data were applied to calculate accumulation rates.

3.2. Calcareous Nannofossil Biostratigraphy

Index species used for Eocene biostratigraphic assignments are rare in cores from U1510 (Data Set S3), and semi-quantitative counts on specific taxa were performed to capture the details of their abundance (Data Set S4). The first occurrence of *Discoaster lodoensis*, which marks the base of Zone NP12 (Martini, 1971; or Zone CNE4 of Agnini et al., 2014), was observed between sample 371-U1510A-52X-3W, 80-80 cm and sample 52X-3W, 95-95 cm (midpoint 477.58 ± 0.07 m CSF-A; Tables S4 and S6). The first occurrence of *Coccolithus crassus* between sample 51X-CCW, 16 cm and sample 51X-CCW (mid-point 468.99 ± 0.09 m CSF-A) denotes the base of Zone CP11 (Okada & Bukry, 1980) and the Top of *Tribrachiatus orthostylus*, between sample 51X-4W, 34 cm and sample 51X-4W, 50 cm (468.63 ± 0.08 m CSF-A), defines the base of Zone NP13 (Martini, 1971; Zone CNE5 of Agnini et al., 2014). Together these two biohorizons serve to biostratigraphically constrain the base of Core 51X. The Base of *Discoaster sublodoensis*, between sample 50X-4W, 31–32 cm and sample 51X-1W, 41-41 (mid-point 462.01 m CSF-A ± 2.60 m) was used to recognize the base of Zone NP14 (Martini, 1971; or base of Zone CNE6 of Agnini et al., 2014) in the upper part of the study section.

In summary, the studied section encompasses Zones NP11 (or CNE3), NP12 (or CNE4), NP13 (or CNE5) to Zone NP14 (or CNE6). Deposition thus occurred from approximately 53.08 to 49.65 Ma and spanned part of the Ypresian (early Eocene).

3.3. Integrated Age Model and Core Recovery

To improve the shipboard age model of Site U1510 in this time window (Sutherland, Dickens, Blum, Agnini, Alegret, Bhattacharya, et al., 2019), we refined the calcareous nannofossil biostratigraphy. Unfortunately, the very weak intensity of paleomagnetic remanence associated with coring disturbance inhibited the use of magnetostratigraphic data and thus the age model is based on the integration of calcareous nannofossil biostratigraphy and isotope stratigraphy. The tie-points used to construct our age model are the Base of *D. lodoensis*, the Top of *T. orthosylus* and the Base of *D. sublodoensis* (Table S1).

Printed by [Icelandair ehf - 185.056.012.142 - /doi/epdf/10.1029/2020PA004179] at [04/08/2021].

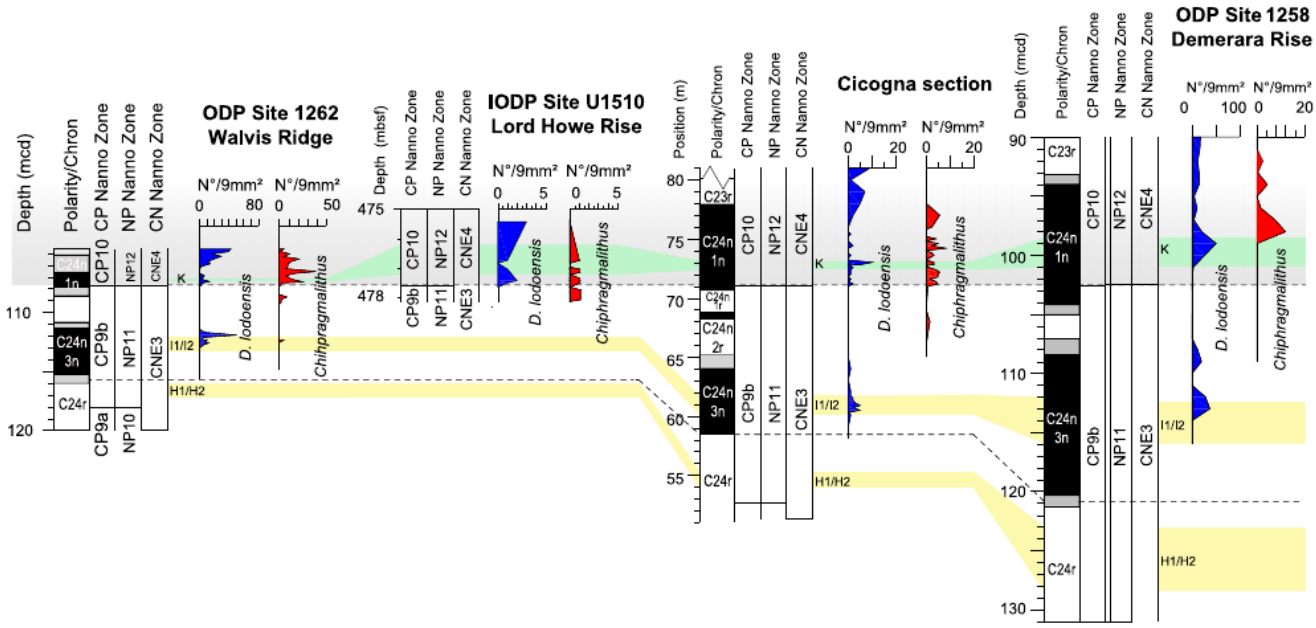

Figure 4. Bio-magnetostratigraphic correlation of the lower part of the studied interval at International Ocean Discovery Program (IODP) Site U1510 with ODP Site 1258 (this study), ODP Site 1262 (Agnini et al., 2007) and Cicogna section (Dallanave et al., 2009). The green interval represents the K event.

Constraining the base of the section was not straightforward because of difficulties in placing the Base of *D. lodoensis*, which shows a discontinuous record especially if core recovery is poor (Agnini et al., 2014, 2016), published data sets are qualitative and not quantitative, or the calcareous nannofossil taxa are very rare (Slotnick et al., 2012; Dallanave et al., 2015). The reason for this is the peculiar abundance pattern characterized by a first presence (B) coinciding with I1-I2 events followed by a virtual absence (ca. 500 kyr; Westerhold et al., 2017) and eventually, the first common and continuous occurrence of this taxon (Bc) (Figure 4). To disentangle this issue, we analyzed the abundance of *Chiphragmalithus* spp., which appears at the base of the study section. The comparison of our data set with those available from ODP Site 1262 (South Atlantic), the Cicogna on-land section in the Tethys Ocean (Agnini et al., 2007, 2016; Dallanave et al., 2009), and new data from ODP Site 1258 (equatorial Atlantic) allow for a global correlation (Figure 4). The bio-magnetostratigraphic framework provides a straightforward correlation with Site U1510: the simultaneous occurrence of *D. lodoensis* and *Chiphragmalithus* spp. occurs only after the I1-I2 events, supporting the hypothesis that the first occurrence of *D. lodoensis* at Site U1510 is correlative with the Bc of this taxon. Consequently, the hyperthermal event documented between 477.4 and 476.46 m CSF-A is the K event (Figure 4).

The age model developed for Core U1510-51X is based on the closely spaced Top of *T. orthostylus* and Base of *C. crassus* observed at the base of the core, and the Base of *D. sublodoensis* recognized in Core U1510-50X (Table S1).

Biostratigraphic and carbon isotope data from Site U1510 have been correlated with the composite isotope curve and the bio-magnetostratigraphic framework available from the South Atlantic ODP Sites 1262, 1263, and 1267 (Walvis Ridge) and the equatorial Atlantic ODP Site 1258 (Demerara Rise) (Figure 5). Such correlation supports the view that the lower CIE is the K event (C24n.1nH1), while the tail of the CIE documented at the base of Core U1510-51X is tentatively the S event (C22rH3) (Westerhold et al., 2017, 2018).

The refined biostratigraphic age model for Site U1510 allows for estimates of sedimentation rates, which slightly increase up-section from 4.1 m/Myr across Core U1510-52X to 4.7 m/Myr across Core U1510-51X. These values are consistent with a pelagic-hemipelagic setting of this site during the early Eocene.

Low core recovery across the studied interval (51% and 47% in Cores U1510-51X and U1510-52X, respectively) raises two issues: (a) Are there any unconformities or non-recovery intervals? (b) What sediments are missing, and why? The first issue can partly be solved by observations of core continuity, and second by correlation with drilling rate of penetration (ROP). The CSF scale cannot easily be matched to the DSF (depth

Printed by [Icelandair ehf - 185.056.012.142 - /doi/epdf/10.1029/2020PA004179] at [04/08/2021].

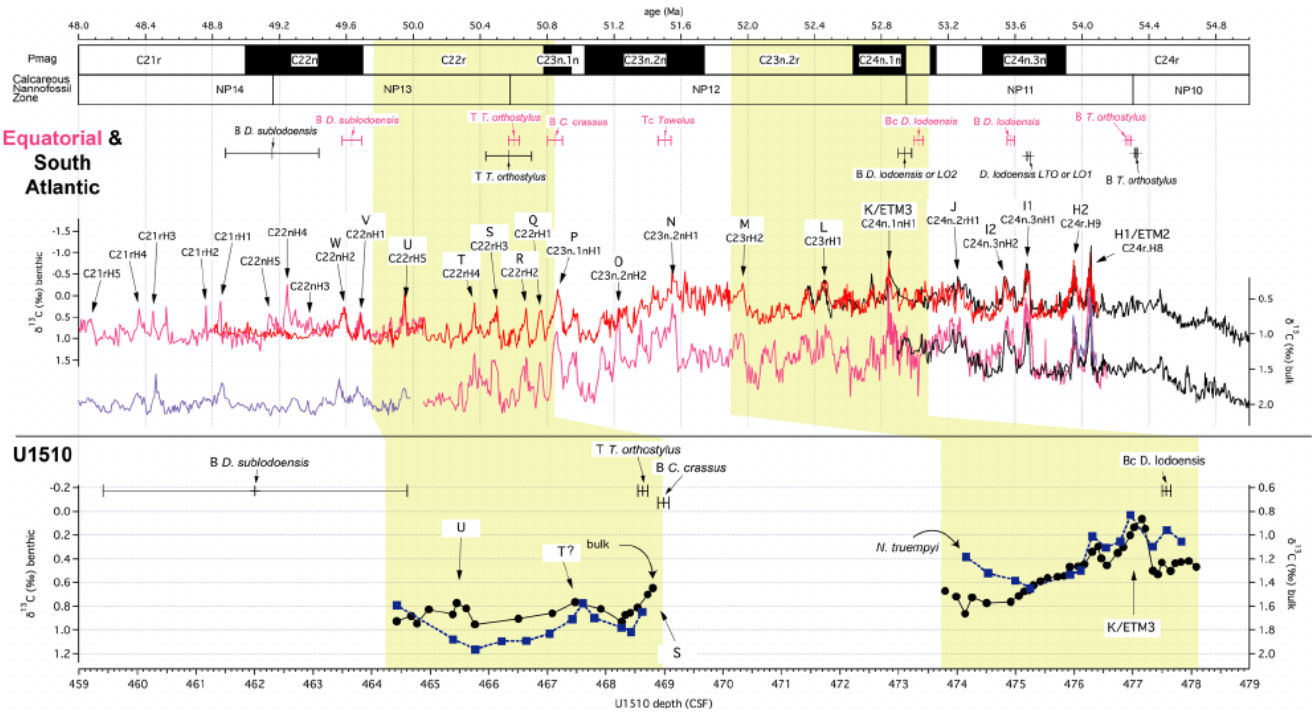

Figure 5. Correlation of Site U1510 with the composite isotope curve and the bio-magnetostratigraphic framework available from the South Atlantic. Top panel: South Atlantic International Ocean Discovery Program Sites 1258 (pink), 1262 (black), 1263 (red) and 1265 (blue) bio- and magnetostratigraphic data as well as benthic and bulk stable isotopes on astrochronology (from Westerhold et al., 2017). Lower panel: U1510 calcareous nannofossil events, benthic and bulk stable isotopes (all this study) and a* ratio (Sutherland, Dickens, Blum, Agnini, Alegret Bhattacharya, et al., 2019) against depth. Yellow intervals show our interpretation of the range cored in U1510 based on calcareous nannofossil assemblages, stable isotopes and an average sedimentation rate.

below seafloor) scale due to poor core recovery, and ROP does not resolve each individual hyperthermal, but it does show a good correlation with the K event in that drilled interval (Figure 6). Reduced ROP indicates reduced recovery, which is consistent with a small unconformity overlying the K event, as suggested by abrupt positive shifts in oxygen isotope values. The second issue is related to the presence of chert, which

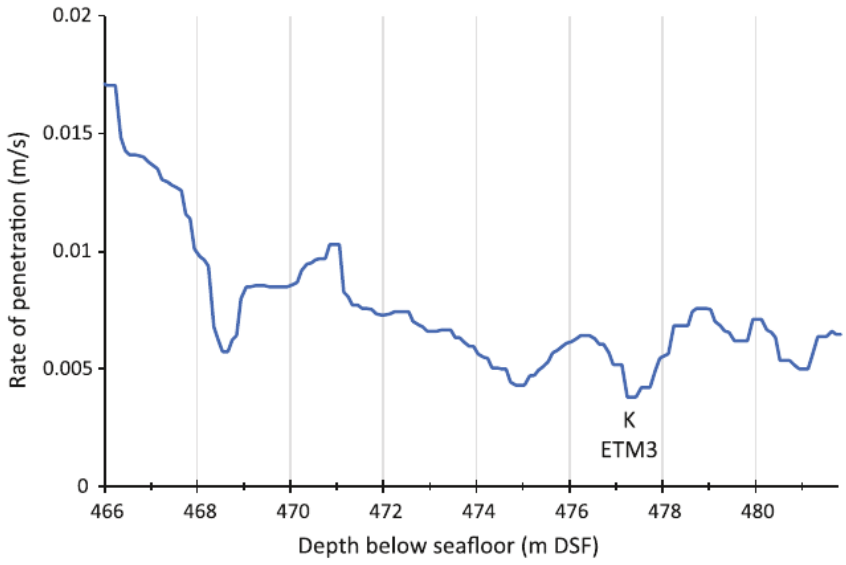

Figure 6. Drilling rate of penetration (ROP) plotted against depth below seafloor (DSF) at Hole 1510A.

Printed by [Icelandair ehf - 185.056.012.142 - /doi/epdf/10.1029/2020PA004179] at [04/08/2021].

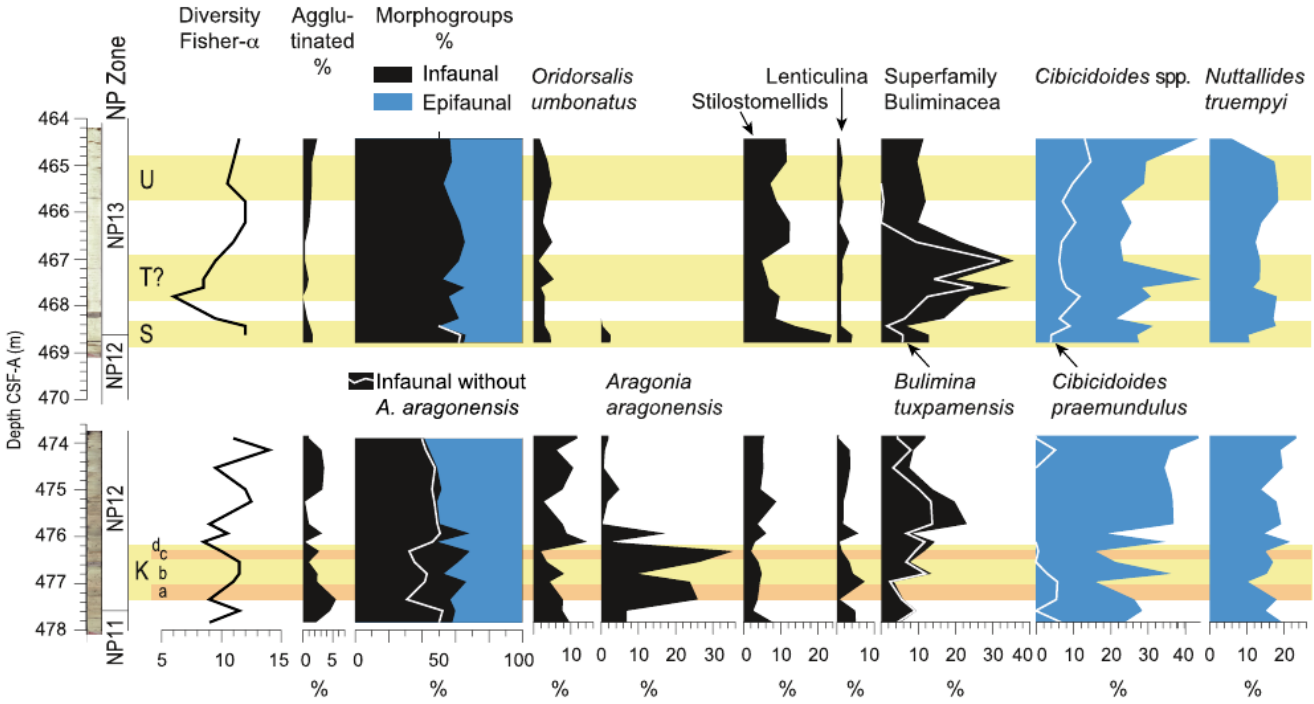

Figure 7. Benthic foraminifera diversity and relative abundance of selected groups and species across the early Eocene at Site U1510, plotted against depth.

blocked the XCB bits during drilling at Site U1510. This might explain why the early part of event S is missing as it corresponds to section U1510-51X-CC, where chert nodules were reported (Sutherland, Dickens, Blum, Agnini, Alegret, Bhattacharya, et al., 2019).

3.4. Identification of Other Eocene CIEs at Site U1510

Other than the K event (~52.4 Ma), the upper part of the S event (~50.4 Ma) and the T (~50.37 Ma) and U (~49.95 Ma) events (Lauretano et al., 2015; or C22rH3, C22rH4 and C22rH5 according to the nomenclature by Westerhold et al., 2017) can be tentatively identified in Core U1510-51X coinciding with bulk carbonate $\delta^{13}C$ minima at 468.80, 467.47, and 465.45 m CSF-A (Figure 5) and coeval decreases in $\delta^{18}O$. Only the recovery portion of event S is captured in the base of Core U1510A-51X, coeval with a peak in a* (Figure 2). Likewise, increased MS toward the upper part of the tentative U event indicates slightly increased terrigenous content. The lack of changes in a* and MS for postulated T event suggests that the identification of this event is less certain than for S and U; alternatively, carbonate dissolution or dilution may have been less prominent than during the S and U events.

Other reasonably prominent events in other records, such as L and M, do not obviously manifest at Site U1510 (Figure 5). Noteworthy, this depth interval at Site U1510 was drilled with XCB, and the total length of recovered core is much less that the downward advance of drilling. Sedimentary expression of these events could very likely exist in core gaps.

4. Faunal Turnover

4.1. Benthic Foraminiferal Assemblages

Assemblages are moderately diverse (mean Fisher-α = 10.7) and dominated by calcareous taxa, with agglutinated species typically making up less than 5% of an assemblage (Figure 7). Diversity fluctuates in the lower half of the studied record (mean Fisher-α = 10.8), with minimum values at 467.8 m CSF-A (Fisher-α = 6) and a gradual recovery upwards (Fisher-α = 11.5–12). Assemblages are composed of mixed morphogroups, with infaunal taxa (e.g., buliminids, stilostomellids) slightly more abundant than epifaunal taxa

Printed by [Icelandair ehf - 185.056.012.142 - /doi/epdf/10.1029/2020PA004179] at [04/08/2021].

(e.g., *Cibicidoides* spp., *N. truempyi*). Overall, assemblages underwent minor and/or gradual changes across the studied section, with intervals of more significant change superimposed. Here we summarize the main assemblage changes across the CIEs that define the four hyperthermals identified at Site U1510 (K, S, T, and U) (Figure 7). The interval corresponding to the K event has been subdivided into four subintervals (a–d) based on changes in microfossil assemblages and on the two negative CIEs that mark the event.

The K event, from 477.4 to 476.2 m CSF-A, is characterized by two marked peaks in the percentage of *Aragonia aragonensis* (up to 35.4% of the assemblages) in subintervals a and c, coinciding with low abundance of *O. umbonatus* and *Lenticulina* spp., and a slight decrease in % *N. truempyi*. The lowermost sample of this interval (subinterval a) contains poorly preserved foraminiferal tests, and agglutinated taxa reach their maximum abundance, which is low (up to 5% of the assemblages). Preservation improves across the rest of event K, as the abundance of agglutinated species gradually decreases.

The relative abundances of *Bulimina tuxpamensis* and other buliminids increase above the K event, followed by a gradual increase in diversity and in % *O. umbonatus* and epifaunal taxa (e.g., *Cibicidoides* spp., *N. truempyi*), which reach their maximum percentage toward 473.79 m CSF-A.

The S event, from 468.61 to 468.3 m CSF-A, contains the highest percentage of stilostomellids (up to 23.6% of the assemblages) and a significant decrease in the percentage of *N. truempyi*.

The T event, from 467.9 to 466.9 m CSF-A, is characterized by a marked peak in the percentage of *Bulimina tuxpamensis* (31.8%), which became dominant among buliminid species. The minimum diversity value (Fisher-$\alpha = 6$) is recorded in this interval and assemblages are dominated by buliminids and *Cibicidoides* spp. (up to 35% and 40% of the assemblages, respectively). Their relative abundance decreases, and diversity values recover above this interval.

The U event, from 465.7 to 464.8 m CSF-A, is not marked by significant turnover among benthic foraminifera, possibly due to the low resolution of our study in this part of the record. It is characterized by a high relative abundance of *N. truempyi*. The percentage of this species declines above this interval, coeval with an increase in *Cibicidoides praemundulus*, among other *Cibicidoides* species.

Statistical analyses of benthic foraminiferal assemblages, including Q-mode Detrended Correspondence Analysis (Figure 8) and hierarchical cluster analysis (Figure S4) clearly differentiate samples from the K event, dominated by *A. aragonensis*, from samples where this species is very scarce to absent. The relative abundance of this species controls the distribution of samples along Axis 1 in the DCA analysis (Figure 8) while the distribution of samples along Axis 2 is controlled by the abundance of *B. tuxpamensis*.

4.2. Calcareous Nannofossil Assemblages

Calcareous nannofossil assemblages underwent both long- and short-term changes, the most important being the turnover in abundance between *Toweius* and *Reticulofenestra*. Core U1510-52X is characterized by the relatively high abundance (up to 30.6%) of the genus *Toweius*, which decreases to ~8% at the base of Core 51X (468.87 m CSF-A) and only sporadically occurs above this level. The abundance of *Reticulofenestra* displays an opposite trend, being scarce in Core 52X and becoming dominant (max 38.5%) throughout Core 51X (Figure 9). In addition to this major change in the assemblages, calcareous nannofossils show turnover that is here described across the four main intervals that correspond to the main CIEs:

The K event exhibits a stepped assemblage turnover. Subintervals a and c are characterized by the increase in relative abundance of *Toweius, Chiasmolithus*, and *Sphenolithus* and by a decrease in *Coccolithus* and *Discoaster*, with less marked changes across subinterval c. The opposite pattern is observed in subinterval b, together with an increase in *Zygrhablithus*. Assemblages start to return to background conditions in subinterval d, and full recovery is observed by 476.2 m CSF-A.

The S event coincides with the *Toweius- Reticulofenestra* turnover, and the genera *Coccolithus* and *Discoaster* display relatively high abundances.

The T event assemblages are dominated by *Reticulofenestra* and *Zygrhablithus*. Floral changes are similar to but less intense than those observed across the K event, and unfortunately the low resolution of our study across this interval does not allow the recognition of all the details described for the K event. *Coccolithus,*

Printed by [Icelandair ehf - 185.056.012.142 - /doi/epdf/10.1029/2020PA004179] at [04/08/2021].

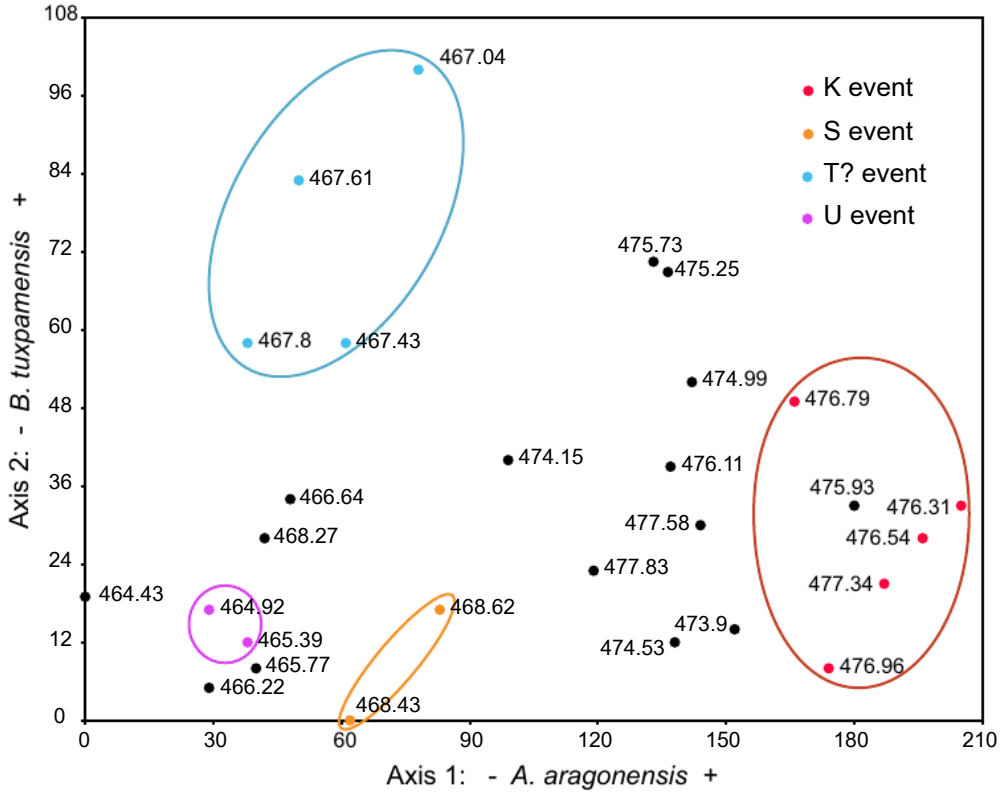

Figure 8. Q-mode (samples) Detrended Correspondence Analysis (DCA) of benthic foraminiferal assemblages from Site U1510.

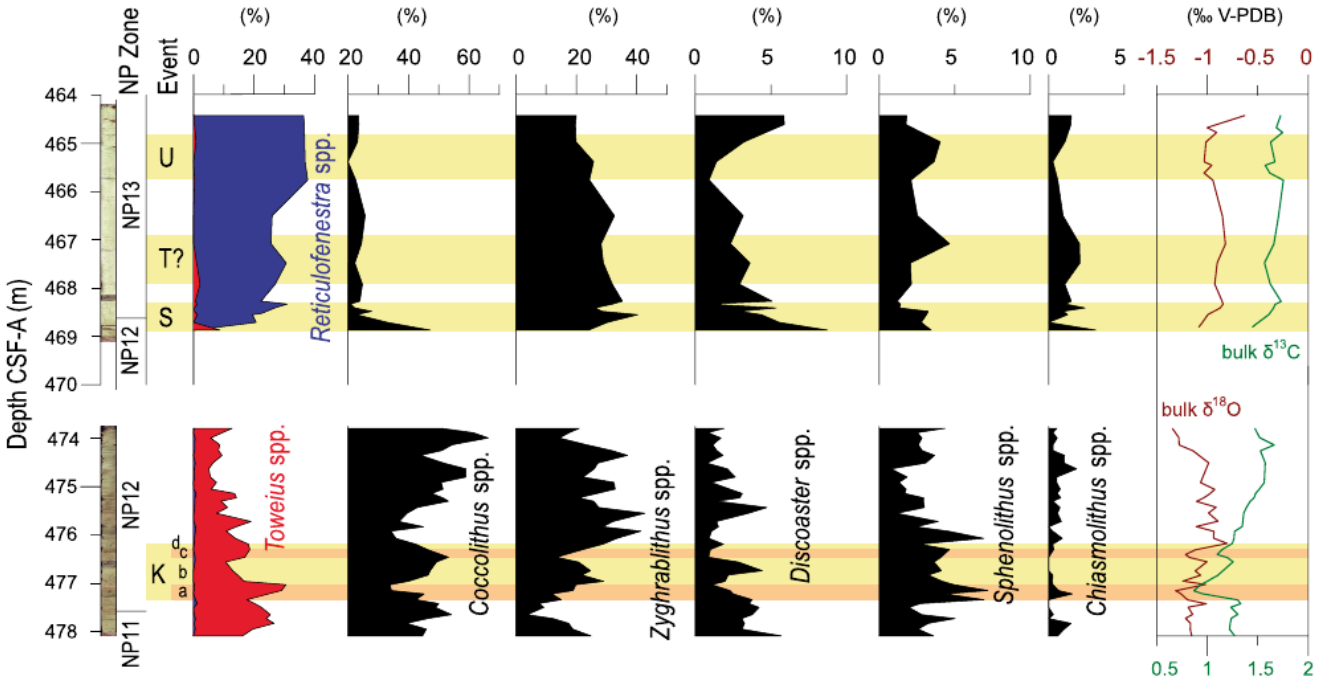

Figure 9. Most relevant calcareous nannofossil taxa from Site U1510 and bulk sediment stable isotopes, plotted against depth.

Printed by [Icelandair ehf - 185.056.012.142 - /doi/epdf/10.1029/2020PA004179] at [04/08/2021].

Sphenolithus and *Zygrhablithus* slightly decrease toward the beginning of the event, and their abundance recovers toward its upper part. The abundance of *Chiasmolithus* is higher than in the K event.

The U event is characterized by the dominance of *Reticulofenestra*. Changes in the relative abundance of *Coccolithus, Discoaster, Sphenolithus*, and *Zygrhablithus* display a similar general pattern as observed across the T interval.

5. Interpretation and Discussion

5.1. The Early Eocene Climatic Optimum in the Tasman Sea and Global Correlation

Correlation to carbon isotope curves from the South Atlantic, which have an excellent bio-magneto-stratigraphic framework (Figure 5), suggests that the bulk carbonate $\delta^{13}C$ minima centered at 477.15, 468.80, 467.47, and 465.45 m CSF-A coincide with the K (~52.4 Ma), S (~50.4 Ma), T (~50.37 Ma), and U (~49.95 Ma) events (Lauretano et al., 2015; Westerhold et al., 2017). The CIEs are associated with OIEs, and this is consistent with some link between global warming and the release of ^{13}C-depleted carbon to the ocean-atmosphere system (Dickens et al., 1995, 1997). Additionally, increasing carbonate $\delta^{13}C$ up section suggests part of the study interval coincides with the positive carbon isotope shift in the middle of the EECO (Luciani et al., 2016; Westerhold et al., 2017). Noteworthy, the relatively high carbonate content at Site U1510, including across the CIEs, suggests the record is less affected by seafloor carbonate dissolution than most published sites in the Pacific and in the Atlantic Oceans, many of which lie at deeper paleodepths.

A succession of CIEs, including the four discussed here, have been recognized in marine bulk carbonate records from the Atlantic (e.g., ODP Sites 1258 and 1265, Westerhold et al., 2018; and ODP Site 1263, Thomas et al., 2018). Some of them have been documented in deep-sea sequences from the Pacific (DSDP Site 577, Cramer et al., 2003; ODP Site 1209, Bhattacharya & Dickens, 2020; Westerhold et al., 2018) and uplifted marginal sections from New Zealand (Branch Stream and Mead Stream sections in the Clarence Valley, Slotnick et al, 2015; and mid-Waipara River, Canterbury Basin, Crouch et al., 2020). At least two distinct CIEs mark the bulk carbonate $\delta^{13}C$ record across the K event at Site U1510 and elsewhere, but the magnitude is smaller than in records from the Atlantic (e.g., Sites 1258 and 1263; Westerhold et al., 2017; Thomas et al., 2018), which display $\delta^{13}C$ decreases of 0.8‰–1.0‰ for the event, and slightly lower than in records from the central north Pacific (−0.5‰ at DSDP Site 577; Cramer et al., 2003) and New Zealand sections (−0.6‰ to −0.5‰; Crouch et al., 2020; Slotnick et al., 2015). The second step of the K event at Site U1510 is equivalent in magnitude to that observed at Pacific Site 1209 (−0.2‰; Bhattacharya & Dickens, 2020). The benthic foraminifera CIE associated with the K event at Site U1510 (−0.3‰) is lower than that recorded at Pacific Site 865 (−0.6‰; Bralower, Parrow, et al., 1995; Bralower, Zachos, et al., 1995; Katz et al., 2003), and the difference is more pronounced compared to that at Atlantic Site 1262 (−0.9‰; Thomas et al., 2018).

In summary, the bulk carbonate CIEs associated with the K event at Site U1510 are similar to or slightly smaller than those recorded in other Pacific records, and significantly smaller than in Atlantic records. The same is true for the CIEs in benthic foraminifera. This contrasting behavior continues for subsequent events. South Atlantic bulk carbonate $\delta^{13}C$ records (i.e., ODP Sites 1258 and 1265) show CIE magnitudes of approximately −0.6‰, −0.4‰, and −0.3‰ for the S, T, and U events, respectively, whereas the Site U1510 record displays magnitudes roughly half of these. Interestingly, early Eocene bulk carbonate $\delta^{13}C$ from nearby mid-Waipara River displays CIE magnitudes more consistent with South Atlantic sites (i.e., negative shifts of 0.5‰–1.0‰ for the listed excursions; Crouch et al., 2020), though these events are only tentatively correlated for the section. The inter-site differences in excursion magnitude described above may be related to the lower resolution of the U1510 and 1209 records, but the question remains why bulk and benthic foraminiferal CIEs across the K event are consistently smaller in Pacific records compared to Atlantic records.

Chert is exceptionally common in early Eocene deep-sea sedimentary records from the North Atlantic (Penman et al., 2019; Witkowski et al., 2020) and from now-uplifted sections of the Tethys region (Monechi & Thierstein, 1985). In the oligotrophic early Cenozoic oceans, biosiliceous sedimentation was likely facilitated by terrestrial supply of dissolved silicon along continental margins (Witkowski et al., 2020). Enhanced silicate weathering during hyperthermal events, combined with a circulation-driven focusing of silica burial, has been suggested as a common formation mechanism of chert deposits associated with hyperthermal events in the Atlantic Ocean, but so far the association of biosiliceous sediments and early Eocene

Printed by [Icelandair ehf - 185.056.012.142 - /doi/epdf/10.1029/2020PA004179] at [04/08/2021].

hyperthermal events has not been reported from the Pacific Ocean (Penman et al., 2019). Interbedding of cherty layers greatly affected drilling and core recovery during IODP Expedition 371. Reductions in ROP in Eocene sediments at Site U1510 were associated with chert nodules that slowed drilling, damaged XCB drill bits and plugged the core collection aperture (leading to poor core recovery). One might speculate that the occurrence of chert nodules in the early part of event S at Site U1510 might result from elevated silica burial during hyperthermal events, although this interpretation contradicts evidence from Clarence valley sites at same paleolatitude where chert is absent from hyperthermal intervals (Slotnick et al., 2015). We acknowledge that further investigation lies beyond the scope of the present study, and further studies are needed to look into the distribution of chert layers with climate significance across hyperthermal events at sites drilled in the Tasman Sea during IODP Expedition 371.

5.2. Biotic and Paleoenvironmental Consequences of Early Eocene Hyperthermals

5.2.1. Deep Seafloor

Moderate diversity of benthic foraminiferal assemblages and a mixed morphogroup composition indicate oligo-mesotrophic conditions at the seafloor, in a setting located well above the CCD as inferred from the strong dominance of calcareous taxa (Figure 7).

Diversity fluctuates but shows no significant changes across the K event, which includes the largest CIE (0.4‰) followed by a minor one (~0.2‰). Calcareous tests from the lower part of the K event are poorly preserved, but several lines of evidence suggest there was no significant $CaCO_3$-dissolution at the seafloor during this hyperthermal: high % $CaCO_3$ content, dominance of calcareous tests (95% of the assemblages), and lack of abundance peaks of $CaCO_3$ corrosion-resistant species that thrived during the PETM, such as *Lenticulina*, *O. umbonatus* or *N. truempyi* (Alegret et al., 2018; Alegret, Ortiz, Orue-Etxebarria, et al., 2009; Alegret, Ortiz & Molina, 2009; Nguyen et al., 2009) (Figure 7). This is consistent with results from the equatorial Pacific (Arreguín-Rodríguez et al., 2016) and the South Atlantic Ocean, where more muted faunal changes at deeper, abyssal settings than at shallower (lower bathyal) ones suggest that carbonate dissolution was not the most important cause of the faunal turnover across the K event (Thomas et al., 2018). The most striking feature of the K event is the increased abundance of *A. aragonensis*. This species became more abundant in the deep sea after the peak-PETM (Alegret et al., 2021; Alegret, Ortiz, Orue-Etxebarria, et al., 2009; Alegret, Ortiz & Molina, 2009; Arreguín-Rodríguez et al., 2016; Giusberti et al., 2009; Thomas, 2003) and during other Paleogene hyperthermal events (Alegret et al., 2016; Ortiz et al., 2011), including the K event (Arreguín-Rodríguez et al., 2016), and is thought to have been an opportunistic taxon (Steineck & Thomas, 1996) that proliferated during warm intervals but not under carbonate corrosive conditions (Arreguín-Rodríguez et al., 2016). This interpretation is supported by the peak occurrence of *A. aragonensis* in coincidence with the two negative CIEs and OIEs in subintervals a and c at Site U1510, which are separated by a transient return to background conditions (subinterval b).

Interpretations regarding export productivity across the K event are not straightforward. The relative abundance of morphogroups fluctuates between 50% and 68% but does not show significant changes as compared to the sediments below and above the event (Figure 7). These percentages indicate mixed infaunal-epifaunal morphogroups (mesotrophic conditions according to Jorissen et al., 2007) or a slightly higher percentage of infaunal ones (increased food supply to the seafloor). But this interpretation is at odds with the common occurrence of the oligotrophic species *N. truempyi* (e.g., Nomura, 1995; Thomas et al., 2000) and with the low abundance of buliminid taxa, which are common at locations with an abundant food supply (e.g., Fontanier et al., 2002; Gooday, 2003). The infaunal *A. aragonensis* is an extinct species and its paleoecological interpretation is uncertain, but its higher abundance during the K event and other hyperthermals may have been related to warmer temperatures rather than to its preference for eutrophic conditions (as expected for an infaunal taxon). The marked increase in % *A. aragonensis* across the K event at Site U1510 is consistent with the interpretation of an opportunistic behavior of this species during warming events. In fact, its abundance strongly influences the distribution of samples in the Q-mode DCA analysis (Figure 8) and in the hierarchical cluster analysis (Figure S4). The question remains, what would the assemblages look like if *A. aragonensis* had not behaved as an opportunistic species and increased in abundance far beyond its usual rare occurrences (Alegret et al., 2021) in the deep sea? If the percentage of *A. aragonensis* is substracted from the total %infaunal morphogroups, epifaunal taxa (up to 70% of the assemblages),

Printed by [Icelandair ehf - 185.056.012.142 - /doi/epdf/10.1029/2020PA004179] at [04/08/2021].

which are better adapted to a low food supply (Jorissen et al., 2007), become more abundant than infaunal ones (30%) during the K event. This morphogroup composition, and the occurrence of common oligotrophic taxa, point to a slightly more oligotrophic scenario than the background oligo-mesotrophic conditions. We further hypothesize that the abundance peaks of *A. aragonensis* suggest that this infaunal species was able to cope with oligotrophic conditions at the seafloor and thrive under high temperatures. Warming may have enhanced remineralization of organic matter throughout the entire water column (Ma et al., 2014) and decreased the food delivery to the seafloor, as proposed for South Atlantic ODP Site 1263 across the K event (Thomas et al., 2018). At Pacific Ocean Site 865, a moderate increase in export productivity was inferred across the K event, but the depositional setting of that site, atop a submarine seamount, was significantly different and possibly controlled by trophic focusing (Arreguín-Rodríguez et al., 2016), thus not readily comparable to Site U1510.

The percentage of *A. aragonensis* decreases and the relative abundance of most taxa recover after the K event, but the abrupt positive shift in $\delta^{18}O$ values suggests an unconformity at the top of this event, thus its immediate aftermath has not been recorded at Site U1510. Lower remineralization of organic matter in the water column under cooler temperatures (Ma et al., 2014) may have contributed to the recovery of food supply and the return to the pre-K oligo-mesotrophic conditions, as evidenced by assemblages with mixed epifaunal—infaunal morphogroups.

Less intense hyperthermal events have been identified in the upper part of our record (Core 51X). The recorded (upper) part of S event is characterized by the highest abundance of stilostomellids, an extinct group of cylindrical taxa that have been interpreted as shallow infaunal suspension feeders that extended their pseudopods through their complex aperture, and which had a low metabolism (Hottinger, 2000, 2006; Mancin et al., 2013). Their proliferation likely reflects enhanced delivery of organic particles to the suspension feeding benthos due to higher current activity. This is supported by a slight increase in %CF, which reaches the maximum value (5.2%) in this interval (Figure 3). A similar but more pronounced pattern was described atop Allison Guyot Site 865 during the PETM and the K event (Arreguín-Rodríguez et al., 2016). Changes in deep water circulation (e.g., Hague et al., 2012; Thomas, 2004; Thomas et al., 2008), including the migration of deep waters sourced from the Southern Ocean toward the tropical Pacific during the Paleogene (Huck et al., 2017; Thomas et al., 2018), may have contributed to enhanced current activity in the central Pacific, especially atop seamount settings (Site 865), and to a minor extent at Site U1510. Additionally, transient reversals in the pattern of deep-ocean circulation during abrupt hyperthermals like the S event affected regional SiO_2 burial patterns and may have significantly contributed to biosiliceous deposition, even to a larger extent than enhanced weathering, as argued for other hyperthermal events (Penman et al., 2019).

The largest decrease in benthic foraminiferal diversity at Site U1510 is associated with the postulated T event, and not with the largest CIE, which marks the K event. Low-diversity is likely related to high dominance of the species *B. tuxpamensis* and *Cibicidoides* spp. across the event. The former taxa increased in abundance in post-PETM assemblages in the NE Atlantic Ocean (DSDP Site 401, D'haenens et al., 2012; Zumaia section, northern Spain, Alegret, Ortiz, Orue-Etxebarria et al., 2009). *B. tuxpamensis* is also common among the post-PETM survivors in lower bathyal to abyssal sites from the central Pacific (1209, 1210, 1211, 1212; Takeda & Kaiho, 2007) and North Pacific Ocean (Site 1220; Kawahata et al., 2015). In the modern oceans, buliminid taxa tolerate reduced oxygen concentrations (e.g., Bernhard et al., 1997; Sen Gupta & Machain-Castillo, 1993), but their high relative abundance is linked to an abundant and fairly continuous food supply (e.g., Fontanier et al., 2002; Gooday, 2003). Given the lack of evidence for reduced oxygen concentrations at Site U1510, such as dark, organic-rich, laminated sediment or small-sized benthic foraminifera, the high abundance of the Superfamily Buliminacea (36% of the assemblages) points to increased export productivity during the T event.

No significant turnover has been observed among benthic foraminifera across the U event. Possibly, this is due to the low resolution of our study in this part of the record.

5.2.2. Surface Waters

Calcareous nannofossil assemblages fluctuate in relative abundance throughout the study section but do not show significant changes in the extinction or speciation rates. This result is consistent with the hypothesis

Printed by [Icelandair ehf - 185.056.012.142 - /doi/epdf/10.1029/2020PA004179] at [04/08/2021].

that calcareous nannofossils are less sensitive than other plankton groups during less extreme paleoclimatic or paleoceanographic events (e.g., the middle/late Eocene turnover; Newsam et al., 2017).

The first turnover coincides with the K event. A peak in abundance of *Toweius* and sphenoliths is observed at its base (subinterval a) (Figure 9). The former taxon is relatively fragile, and its high abundance in coincidence with the negative CIE suggests little to absent $CaCO_3$ dissolution in surface waters during this phase. *Toweius* and *Reticulofenestra* are generally considered temperate/mesotrophic cosmopolitan taxa, *Chiasmolithus* has a colder/more eutrophic affinity and taxa that are usually thought to be warm/oligotrophic include *Coccolithus, Discoaster, Sphenolithus*, and *Zygrhablithus* (e.g., Agnini et al., 2007; Bralower, 2002; Gibbs et al., 2006; Haq & Lohmann, 1976; Monechi et al., 2000; Persico & Villa, 2004; Villa et al., 2008, 2014; Wei & Wise, 1990). Based on this rationale, the increase in *Toweius* and *Chiasmolithus* at the base of the K event (subinterval a) likely indicates more eutrophic conditions during this warming interval. The peak in *Sphenolithus* is rather controlled by warmer waters, and this is consistent with the idea that the more negative $\delta^{13}C$ values coincide with the peak in warmth. The decrease in *Coccolithus* and *Discoaster* also supports enhanced eutrophication. Opposite changes in subinterval b point to a recovery phase characterized by more oligotrophic conditions. *Zygrhablithus bijugatus* may have been controlled either by nutrient availability (high abundance during oligotrophic phases) or by $CaCO_3$ water saturation (Kelly et al., 2005; Rivero-Cuesta et al., 2019), as documented across the PETM (Agnini et al., 2016; Penman, 2016). Assemblages suggest the return to relatively more eutrophic conditions across subinterval c, and to pre-K conditions in subinterval d. The exception to this is the high relative percentages of *Zygrhablithus*, whose abundance is likely related to the carbonate oversaturation that typically follows hyperthermals (Gibbs et al., 2012; Penman, 2016).

The S event coincides with one of the major changes in calcareous nannofossil assemblages of the entire Cenozoic, when the reticulofenestrids first appeared and outcompeted the rest of taxa (Figure 9), mainly their counterpart *Toweius* (Agnini et al., 2006; Cappelli et al., 2019; Schneider et al., 2011), and *T. orthostylus* went extint. The peak in *Discoaster* in the lowermost sample from Core U1510-51X is followed by the remarkable increase in *Reticulofenestra*, pointing to a shift from warm/oligotrophic to cooler/mesotrophic conditions and a possible gradual/partial destratification of the global ocean (Cappelli et al., 2019; Schneider et al., 2011). Since these major assemblage changes occurred during the long-term Eocene cooling documented in the global isotope stack (e.g., Westerhold et al., 2020), we speculate that ocean circulation may have changed during the S event, leading to long-term changes in surface waters. The high abundance of *Discoaster* during the EECO suggests warm and highly stratified sea surface waters, thus less intense global circulation. This was followed by enhanced ocean circulation and increased mixing of surface waters (destratification), as supported by the global onset and successive dominance of mesotrophic taxa (i.e., reticulofenestrids). Regarding the timing of the *Reticulofenestra/Toweius* turnover, the data available (e.g., Agnini et al., 2006; Cappelli et al., 2019; Crouch et al., 2020; Dallanave et al., 2015; Schneider et al., 2011) suggest a scenario in which the onset of *Reticulofenestra* first appeared in Zone NP12 at high latitudes, and entered the record later at mid- and low latitudes.

The T and U events display assemblage changes that are similar to those observed during the K event, although their smaller magnitude and the lower resolution of our study partially inhibit observation of the articulation visible across the K event. The increase in *Reticulofenestra* points to increased nutrient availability.

In brief, calcareous nannofossils from Site U1510 indicate that these events are, at least locally, characterized by increased nutrient availability in surface waters followed by oligotrophic conditions, and eventually by a return to background (pre-event) levels.

5.2.3. Decoupling of the Ocean Response to Early Eocene Hyperthermal Events

We document decoupled responses of calcareous nannofossils and benthic foraminifera across the K event, which point to enhanced eutrophication in surface waters with no clear consequences at the seafloor, where oligo-mesotrophic conditions are inferred. In contrast, assemblages indicate increased surface productivity during smaller hyperthermals S, and T and U, and higher food supply to the seafloor during S, and T events at Site U1510. In the recorded part of event S, planktic assemblages show a shift from warm/oligotrophic to cooler/mesotrophic conditions, a possible gradual/partial destratification of the global ocean and stronger

Printed by [Icelandair ehf - 185.056.012.142 - /doi/epdf/10.1029/2020PA004179] at [04/08/2021].

circulation (as indicated by the replacement of abundant *Discoaster* by *Reticulofenestra*; Cappelli et al., 2019; Schneider et al., 2011). At the seafloor, increased abundance of stilostomellids likely indicates higher current activity that delivered food particles to suspension feeders. These paleoenvironmental changes may support transient reversals in deep-ocean circulation patterns (Penman et al., 2019), possibly combined with enhanced terrestrial supply of dissolved silicon (Witkowski et al., 2020) and likely explain chert nodules in the lower part of the S event at Site U1510. Increased nutrient availability in surface waters was coeval with eutrophic assemblages at the seafloor (dominated by *B. tuxpamensis*) during the T event, but no chert deposits were described or inferred for this interval at Site U1510 (Sutherland, Dickens, Blum, Agnini, Alegret, Bhattacharya, et al., 2019). Alternatively, the location of this site on a ridge near the boundary zone of subtropical and subantarctic waters (equivalent of subtropical front today; Figure 1) might account for the the high productivity recorded by surface-dwellers across the K, S, T, and U events.

To account for the similarities and differences in the planktic-benthic biotic response, one might argue that warming during the K event influenced biological processes and accelerated metabolic rates of benthic foraminifera (Hoegh-Guldberg & Bruno, 2010), which double with a temperature increase of ~10°C (e.g., Gillooly et al., 2001), while the increased food demand of benthic foraminifera was not compensated by increased arrival of nutrients to the seafloor. Even though calcareous nannofossils point to eutrophication in surface waters during the K event, pronounced warming may have enhanced remineralization of organic matter in the water column or even altered transfer efficiency by modifying metabolic rates in the food chain (Boscolo-Galazzo et al., 2021; John et al., 2013, 2014; Ma et al., 2014), thus not resulting in eutrophic conditions in the benthic realm. A similar scenario has been proposed across the K event at South Atlantic ODP Site 1263 (Thomas et al., 2018) and across other Eocene warming intervals such as the Middle Eocene Climatic Optimum (Boscolo-Galazzo et al., 2015) and ETM2 (Jennions et al., 2015), and this mechanism (though at a larger magnitude) is also considered as one of the main causes of starvation and extinction of the deep-sea benthic foraminifera across the PETM (e.g., Alegret et al., 2010, 2021; Thomas, 2007).

We speculate that warming, associated remineralization of organic matter and possibly accelerated metabolic rates among benthic foraminifera attenuated the effects of high surface primary productivity on the trophic signature at the seafloor during the K event but not during smaller hyperthermals S and T, when benthic assemblages point to a sustained food supply to the seafloor. This interpretation is supported by the occurrence of abundant stilostomellids across event S, as this extinct group has been hypothesized to have low metabolic rates (Mancin et al., 2013). Warming triggered a decrease in benthic foraminiferal test size across the PETM (Thomas, 2003; Alegret et al., 2010; Arreguín-Rodríguez et al., 2014) but not across smaller hyperthermal events (Foster et al., 2013), suggesting a threshold for dwarfism was crossed during the largest hyperthermal only. It is widely acknowledged that more severe warming generally results in more severe effects on the biota (e.g., Arreguín-Rodríguez & Alegret, 2016; Arreguín-Rodríguez et al., 2016; Thomas et al., 2018), but further data from comparable settings (e.g., paleodepth, marginality) are needed to establish the correlation between the magnitude of warming, the temperature threshold and the degree of perturbation of benthic foraminiferal assemblages. In addition, the bentho-pelagic coupling may have functioned differently in a greenhouse world with high remineralization of organic carbon in the oceans, where at least part of the food supply to the benthos may have been in the form of dissolved organic matter (Alegret et al., 2021).

6. Conclusions

Eocene sediments recovered during IODP Expedition 371 on southern Lord Howe Rise provide detailed records across part of the EECO and some of its hyperthermal events in the Tasman Sea, offshore New Zealand. Integration of stable isotopic measurements of bulk sediment and benthic foraminifera with biostratigraphic observations from Site U1510, correlated with the composite isotope curve and the bio-magnetostratigraphic framework available from the South Atlantic, allowed us to identify the K event (~52.4 Ma), and to tentatively assign additional negative CIEs to the S (~50.4 Ma), T (~50.37 Ma), and U (~49.95 Ma) hyperthermal events. An open question remains why the magnitude of the CIEs across the K event and seemingly other smaller hyperthermals is consistently smaller in $\delta^{13}C$ records from the Pacific compared to those from the Atlantic.

Printed by [Icelandair ehf - 185.056.012.142 - /doi/epdf/10.1029/2020PA004179] at [04/08/2021].

Benthic foraminifera and calcareous nannofossils underwent changes in relative abundance of taxa across hyperthermal events, and the highest abundance of warm-water species are recorded within the K event. These two microfossil groups show a decoupled response across the K event, with eutrophication in surface waters and relatively starved assemblages at the seafloor, while both groups point to increased surface productivity and food supply to the seafloor during smaller hyperthermals. Even if ocean circulation patterns changed at this boundary zone between subtropical and subantarctic waters, triggering higher primary productivity, we argue that warming during the K event may have accelerated metabolic rates of benthic foraminifera, and that transfer of organic matter in the water column was less efficient, resulting in oligo-mesotrophic benthic assemblages in spite of the higher nutrient availability in surface waters. In contrast, we speculate that this temperature threshold was not crossed during smaller hyperthermals S and T, but the correlation between the magnitude of warming and the degree of perturbation of benthic foraminiferal assemblages needs to be further investigated.

Calcareous nannofossils underwent a significant long-term evolutionary change from the late S event onwards, when the abundance peak of *Discoaster* was followed by the *Toweius-Reticulofenestra* turnover, pointing to a shift from warm/oligotrophic to cooler/mesotrophic conditions and a possible destratification of the ocean. The onset of these changes at ~50.4 Ma may have been coeval with transient, more vigorous bottom water currents atop Lord Howe Rise, as inferred from benthic foraminifera across the S event. The occurrence of chert nodules and layers with climate significance across hyperthermal events at this and other sites drilled during IODP Exp 371 is worth being explored in future studies.

These detailed records of EECO in the Tasman Sea fill a critical early Eocene paleoclimate data gap during a dynamic tectonic interval, and provide new integrated observations of environmental and biotic responses to hyperthermal events.

Data Availability Statement

Data sets for this research are available online (http://doi.org/10.17605/OSF.IO/H43WS).

Acknowledgments
L. Alegret acknowledges funding from project PID2019-105537RB-I00 (Spanish Ministry of Science and Innovation and FEDER funds), and a 2017 Leonardo Grant for Researchers and Cultural Creators, BBVA Foundation. E. Dallanave is supported by Deutsche Forschungsgemeinschaft (DFG) Projektnummer 408178503. C. Newsam was funded by a UKIODP Moratorium Award. The authors are grateful to the Integrated Ocean Discovery Program (IODP) for providing samples and data used in this study. The IODP is sponsored by the U.S. National Science Foundation (NSF) and participating countries under the management of Joint Oceanographic Institutions, Inc. The authors thank Ellen Thomas for thoughtful discussions on the manuscript, Colin Carney for analytical support, and IODP Expedition 371 Scientists and all personnel aboard the R/V JOIDES Resolution on IODP Expedition 371. Map generated with Gplates.

References

Agnini, C., Fornaciari, E., Raffi, I., Catanzariti, R., Pälike, H., Backman, J., & Rio, D. (2014). Biozonation and biochronology of Paleogene calcareous nannofossils from low and middle latitudes. *Newsletters on Stratigraphy*, *47*, 131–181. https://doi.org/10.1127/0078-0421/2014/0042

Agnini, C., Fornaciari, E., Rio, D., Tateo, F., Backman, J., & Giusberti, L. (2007). Responses of calcareous nannofossil assemblages, mineralogy and geochemistry to the environmental perturbations across the Paleocene/Eocene boundary in the Venetian Pre-Alps. *Marine Micropaleontology*, *63*, 19–38. https://doi.org/10.1016/j.marmicro.2006.10.002

Agnini, C., Macrì, P., Backman, J., Brinkhuis, H., Fornaciari, E., Giusberti, L., et al. (2009). An early Eocene carbon cycle perturbation at ~52.5 Ma in the Southern Alps: Chronology and biotic response. *Paleoceanography*, *24*, PA2209. https://doi.org/10.1029/2008pa001649

Agnini, C., Muttoni, G., Kent, D. V., & Rio, D. (2006). Eocene biostratigraphy and magnetic stratigraphy from Possagno, Italy: The calcareous nannofossil response to climate variability. *Earth and Planetary Science Letters*, *241*, 815–830. https://doi.org/10.1016/j.epsl.2005.11.005

Agnini, C., Spofforth, D. J. A., Dickens, G. R., Rio, D., Pälike, H., Backman, J., et al. (2016). Stable isotope and calcareous nannofossil assemblage record of the late Paleocene and early Eocene (Cicogna section). *Climate of the Past*, *12*, 883–909. https://doi.org/10.5194/cp-12-883-2016

Alegret, L., Arreguín-Rodríguez, G. J., Trasviña-Moreno, C. A., & Thomas, E. (2021). Turnover and stability in the deep sea: Benthic foraminifera as tracers of Paleogene global change. *Global and Planetary Change*, *196*, 103372. https://doi.org/10.1016/j.gloplacha.2020.103372

Alegret, L., Ortiz, S., Arenillas, I., & Molina, E. (2010). What happens when the ocean is overheated? The foraminiferal response across the Paleocene-Eocene thermal maximum at the Alamedilla section (Spain). *GSA Bulletin*, *122*, 1616–1624. https://doi.org/10.1130/b30055.1

Alegret, L., Ortiz, S., Arreguín-Rodríguez, G. J., Monechi, S., Millán, I., & Molina, E. (2016). Microfossil turnover across the uppermost Danian at Caravaca, Spain: Paleoenvironmental inferences and identification of the latest Danian event. *Palaeogeography, Palaeoclimatology, Palaeoecology*, *463*, 45–59. https://doi.org/10.1016/j.palaeo.2016.09.013

Alegret, L., Ortiz, S., & Molina, E. (2009). Extinction and recovery of benthic foraminifera across the Paleocene-Eocene Thermal Maximum at the Alamedilla section (Southern Spain). *Palaeogeography, Palaeoclimatology, Palaeoecology*, *279*, 186–200. https://doi.org/10.1016/j.palaeo.2009.05.009

Alegret, L., Ortiz, S., Orue-Etxebarria, X., Bernaola, G., Baceta, J. I., Monechi, S., et al. (2009). The Paleocene-Eocene thermal maximum: New data from the microfossil turnover at Zumaia section. *Palaios*, *24*, 318–328. https://doi.org/10.2110/palo.2008.p08-057r

Alegret, L., Reolid, M., & Vega Pérez, M. (2018). Environmental instability during the latest Paleocene at Zumaia (Basque-Cantabric Basin): The bellwether of the Paleocene Eocene Thermal Maximum. *Palaeogeography, Palaeoclimatology, Palaeoecology*, *497*, 186–200. https://doi.org/10.1016/j.palaeo.2018.02.018

Alegret, L., & Thomas, E. (2009). Food supply to the seafloor in the Pacific Ocean after the Cretaceous/Paleogene boundary event. *Marine Micropaleontology*, *73*, 105–116. https://doi.org/10.1016/j.marmicro.2009.07.005

Anagnostou, E., John, E. H., Edgar, K. M., Foster, G., Ridgwell, A., Inglis, G. N., et al. (2016). Changing atmospheric CO_2 concentration was the primary driver of early Cenozoic climate. *Nature*, *533*, 380–384. https://doi.org/10.1038/nature17423

Printed by [Icelandair ehf - 185.056.012.142 - /doi/epdf/10.1029/2020PA004179] at [04/08/2021].

Arreguín-Rodríguez, G. J., & Alegret, L. (2016). Deep-sea benthic foraminiferal turnover across early Eocene hyperthermal events at Northeast Atlantic DSDP Site 550. *Palaeogeography, Palaeoclimatology, Palaeoecology*, *451*, 62–72. https://doi.org/10.1016/j.palaeo.2016.03.010

Arreguín-Rodríguez, G. J., Alegret, L., Sepúlveda, J., Newman, S., & Summons, R. E. (2014). Enhanced terrestrial input supporting the *Glomospira* acme across the Paleocene-Eocene boundary in Southern Spain. *Micropaleontology*, *60*(1), 43–51.

Arreguín-Rodríguez, G. J., Alegret, L., & Thomas, E. (2016). Late Paleocene-middle Eocene benthic life on a Pacific seamount (Allison Guyot, ODP site 865): Greenhouse climate and superimposed hyperthermal events. *Paleoceanography*, *31*, 346–364. https://doi.org/10.1002/2015PA002837

Aubry, M.-P. (1984). *Handbook of Cenozoic calcareous nannoplankton, book 1, Ortholithae (discoaster)* (p. 263). Micropaleontology Press, American Museum of Natural History.

Aubry, M.-P. (1988). *Handbook of Cenozoic calcareous nannoplankton, book 2, Ortholithae (Holococcoliths, Ceratoliths, Ortholiths and other)* (p. 279). Micropaleontology Press, American Museum of Natural History.

Aubry, M.-P. (1989). *Handbook of Cenozoic calcareous nannoplankton, book 3, Ortholithae (Pentaliths and Other), Heliolithae (Fasciculiths, Sphenoliths and Others).* (p. 279). Micropaleontology Press, American Museum of Natural History.

Aubry, M.-P. (1990). *Handbook of Cenozoic calcareous nannoplankton, book 4, Heliolithae (Helicoliths, Cribriliths, Lopadoliths and other)* (p. 381). Micropaleontology Press, American Museum of Natural History.

Aubry, M.-P. (1999). *Handbook of Cenozoic calcareous nannoplankton, book 5, Heliolithae (Zygoliths and Rhabdoliths)* (p. 368). Micropaleontology Press, American Museum of Natural History.

Backman, J., & Shackleton, N. J. (1983). Quantitative biochronology of Pliocene and early Pleistocene calcareous nannofossils from the Atlantic, Indian and Pacific oceans. *Marine Micropaleontology*, *8*, 141–170. https://doi.org/10.1016/0377-8398(83)90009-9

Barnet, J. S. K., Littler, K., Westerhold, T., Kroon, D., Leng, M. J., Bailey, I., et al. (2019). A high-fidelity benthic stable isotope record of late Cretaceous-early Eocene climate change and carbon-cycling. *Paleoceanography and Paleoclimatology*, *34*, 672–691. https://doi.org/10.1029/2019pa003556

Beerling, D. J., & Royer, D. L. (2011). Convergent Cenozoic CO_2 history. *Nature Geoscience*, *4*, 418–420. https://doi.org/10.1038/ngeo1186

Bernhard, J. M., Sen Gupta, B. K., & Borne, P. F. (1997). Benthic foraminiferal proxy to estimate dysoxic bottom water oxygen concentrations, Santa Barbara Basin, US Pacific continental margin. *Journal of Foraminiferal Research*, *27*, 301–310. https://doi.org/10.2113/gsjfr.27.4.301

Bhattacharya, J., & Dickens, G. R. (2020). Eocene carbonate accumulation in the north-central Pacific Ocean: New insights from ocean drilling program Site 1209, Shatsky Rise. *Sedimentary Geology*, *405*, 105705. https://doi.org/10.1016/j.sedgeo.2020.105705

Bijl, P. K., Bendle, J. A. P., Bohaty, S. M., Pross, J., Schouten, S., Tauxe, L., et al. (2013). Eocene cooling linked to early flow across the Tasmanian Gateway. *Proceedings of the National Academy of Sciences of the United States of America*, *110*(24), 9645–9650. https://doi.org/10.1073/pnas.1220872110

Bijl, P. K., Schouten, S., Sluijs, A., Reichart, G. L., Zachos, J. A., & Brinkhuis, H. (2009). Early Palaeogene temperature evolution of the southwest Pacific Ocean. *Nature*, *461*(7265), 776–779. https://doi.org/10.1038/nature08399

Boscolo-Galazzo, F., Crichton, K. A., Ridgwell, A., Mawbey, E. M., Wade, B. S., & Pearson, P. N. (2021). Temperature controls carbon cycling and biological evolution in the ocean twilight zone. *Science*, *371*, 1148–1152. https://doi.org/10.1126/science.abb6643

Boscolo-Galazzo, F., Thomas, E., & Giusberti, L. (2015). Benthic foraminiferal response to the middle Eocene climatic optimum (MECO) in the Southeastern Atlantic (ODP Site 1263). *Palaeogeography, Palaeoclimatology, Palaeoecology*, *417*, 432–444. https://doi.org/10.1016/j.palaeo.2014.10.004

Bown, P. R. (2005). Palaeogene calcareous nannofossils from the Kilwa and Lindi areas of coastal Tanzania (Tanzania Drilling Project 2003–4). *Journal of Nannoplankton Research*, *27*(1), 21–95.

Bown, P. R., & Young, J. R. (1998). Techniques. In P. R. Bown (Ed.), *Calcareous nannofossil biostratigraphy* (pp. 16–28). Kluwer Academic Publishers. https://doi.org/10.1007/978-94-011-4902-0_2

Bralower, T. J. (2002). Evidence of surface water oligotrophy during the Paleocene-Eocene thermal maximum: Nannofossil assemblage data from ocean drilling program Site 690, Maud rise, Weddell Sea. *Paleoceanography*, *17*(2), 12-1–13-12. https://doi.org/10.1029/2001PA000662

Bralower, T. J., Parrow, M., Thomas, E., & Zachos, J. C. (1995). Data report: Stable isotope stratigraphy of the Paleogene pelagic cap at Site 865, Allison Guyot. In E. L. Winterer, W. W. Sager, J. V. Firth, & J. M. Sinton (Eds.), (Eds), *Proceedings of the ocean drilling Program, science results* (Vol. 143). Ocean Drill. Program.

Bralower, T. J., Zachos, J. C., Thomas, E., Parrow, M., Paull, C. K., Kelly, D. C., et al. (1995). Late Paleocene to Eocene paleoceanography of the equatorial Pacific Ocean: Stable isotopes recorded at Ocean Drilling Program Site 865, Allison Guyot. *Paleoceanography*, *10*, 841–865. https://doi.org/10.1029/95PA01143

Buzas, M. A., Culver, S. J., & Jorissen, F. J. (1993). A statistical evaluation of the microhabitats of living (stained) infaunal benthic foraminifera. *Marine Micropaleontology*, *20*, 311–320. https://doi.org/10.1016/0377-8398(93)90040-5

Cao, W., Zahirovic, S., Flament, N., Williams, S., Golonka, J., & Müller, R. D. (2017). Improving global paleogeography since the late Paleozoic using paleobiology. *Biogeosciences*, *14*(23), 5425–5439. https://doi.org/10.5194/bg-14-5425-2017

Cappelli, C., Bown, P. R., Westerhold, T., Bohaty, S. M., de Riu, M., Lobba, V., et al. (2019). The early-middle Eocene transition: An integrated calcareous nannofossil and stable isotope record from the Northwest Atlantic Ocean (IODP Site U1410). *Paleoceanography and Paleoclimatology*, *34*(12), 1913–1930. https://doi.org/10.1029/2019PA003686

Cook, R. A., Sutherland, R., & Zhu, H. (1999). Cretaceous-Cenozoic geology and petroleum systems of the Great South Basin, New Zealand. (Vol. 20, p. 190). Institute of Geological & Nuclear Sciences.

Cramer, B., Toggweiler, J. R., Wright, J. D., Katz, M. E., & Miller, K. G. (2009). Ocean overturning since the Late Cretaceous: Inferences from a new benthic foraminiferal isotope compilation. *Paleoceanography*, *24*, PA4216. https://doi.org/10.1029/2008PA001683

Cramer, B. S., Wright, J. D., Kent, D. V., & Aubry, M. P. (2003). Orbital climate forcing of $\delta^{13}C$ excursions in the late Paleocene-early Eocene (chrons C24n–C25n). *Paleoceanography*, *18*(4), 1097. https://doi.org/10.1029/2003PA000909

Cramwinckel, M. J., Huber, M., Kocken, I., Agnini, C., Bijl, P., Bohaty, S., et al. (2018). Synchronous tropical and polar temperature evolution in the Eocene. *Nature*, *559*(7714), 382–386. https://doi.org/10.1038.s41586-018-0272-2

Cramwinckel, M. J., Woelders, L., Huurdeman, E. P., Peterse, F., Gallagher, S. J., Pross, J., et al. (2020). Surface-circulation change in the southwest Pacific Ocean across the middle Eocene climatic optimum: Inferences from dinoflagellate cysts and biomarker paleothermometry. *Climate of the Past*, *16*, 1667–1689. https://doi.org/10.5194/cp-16-1667-2020

Crouch, E. M., Shepherd, C. L., Morgans, H. E. G., Naafs, B. D. A., Dallanave, E., Phillips, A., et al. (2020). Climatic and environmental changes across the early Eocene climatic optimum at mid-Waipara River, Canterbury basin, New Zealand. *Earth-Science Reviews*, *200*, 102961. https://doi.org/10.1016/j.earscirev.2019.102961

Printed by [Icelandair ehf - 185.056.012.142 - /doi/epdf/10.1029/2020PA004179] at [04/08/2021].

Dallanave, E., Agnini, C., Bachtadse, V., Muttoni, G., Crampton, J. S., Strong, C. P., et al. (2015). Early to middle Eocene magneto-biochronology of the southwest Pacific Ocean and climate influence on sedimentation: Insights from the Mead Stream section, New Zealand. *The Geological Society of America Bulletin*, *127*, 643–660. https://doi.org/10.1130/b31147.1

Dallanave, E., Agnini, C., Muttoni, G., & Rio, D. (2009). Magnetobiostratigraphy of the Cicogna section (Italy): Implications for the late Paleocene-early Eocene time scale. *Earth and Planetary Science Letters*, *285*, 39–51. https://doi.org/10.1016/j.epsl.2009.05.033

D'haenens, S., Bornemann, A., Stassen, P., & Speijer, R. P. (2012). Multiple early Eocene benthic foraminiferal assemblage and $\delta^{13}C$ fluctuations at DSDP Site 401 (Bay of Biscay—NE Atlantic). *Marine Micropaleontology*, *88–89*, 15–35. https://doi.org/10.1016/j.marmicro.2012.02.006

Dickens, G. R. (2011). Methane release from gas hydrate systems during the Paleocene-Eocene thermal maximum and other past hyperthermal events: Setting appropriate parameters for discussion. *Climate of the Past*, *7*, 1139–1174. https://doi.org/10.5194/cp-7-831-2011

Dickens, G. R., Castillo, M. M., & Walker, J. C. G. (1997). A blast of gas in the latest Paleocene: Simulating first order effects of massive dissociation of oceanic methane hydrate. *Geology*, *25*, 259–262. https://doi.org/10.1130/0091-7613(1997)025<0259:abogit>2.3.co;2

Dickens, G. R., O'Neil, J. R., Rea, D. K., & Owen, R. M. (1995). Dissociation of oceanic methane hydrate as a cause of the carbon isotope excursion at the end of the Paleocene. *Paleoceanography*, *10*, 965–971. https://doi.org/10.1029/95pa02087

D'Onofrio, R., Luciani, V., Dickens, G. R., Wade, B. S., & Kirtland Turner, S. (2020). Demise of the planktic foraminifer genus *Morozovella* during the early Eocene climatic optimum: New Records from ODP Site 1258 (Demerara rise, western Equatorial Atlantic) and Site 1263 (Walvis Ridge, South Atlantic). *Geosciences*, *10*(3), 88. https://doi.org/10.3390/geosciences10030088

Fontanier, C., Jorissen, F. J., Licari, L., Alexandre, A., Anschutz, P., & Carbonel, P. (2002). Live benthic foraminiferal faunas from the Bay of Biscay: Faunal density, composition and microhabitats. *Deep-Sea Research I*, *49*, 751–785. https://doi.org/10.1016/s0967-0637(01)00078-4

Foster, L. C., Schmidt, D. N., Thomas, E., Arndt, S., & Ridgwell, A. (2013). Surviving rapid climate change in the deep-sea during the Paleogene hyperthermals. *Proceedings of the National Academy of Sciences of the United States of America*, *110*, 9273–9276. https://doi.org/10.1073/pnas.1300579110

Galeotti, S., Sprovieri, M., Rio, D., Moretti, M., Francescone, F., Sabatino, N., et al. (2019). Stratigraphy of early to middle Eocene hyperthermals from Possagno (Southern Alps, Italy) and comparison with global carbon isotope records. *Palaeogeography, Palaeoclimatology, Palaeoecology*, *527*, 39–52. https://doi.org/10.1016/j.palaeo.2019.04.027

Gibbs, S. J., Bown, P. R., Murphy, B. H., Sluijs, A., Edgar, K. M., Pälike, H., et al. (2012). Scaled biotic disruption during early Eocene global warming events. *Biogeosciences*, *9*(11), 4679–4688. https://doi.org/10.5194/bg-9-4679-2012

Gibbs, S. J., Bralower, T. J., Bown, P. R., Zachos, J. C., & Bybell, L. M. (2006). Shelf and open-ocean calcareous phytoplankton assemblages across the Paleocene-Eocene Thermal Maximum: Implications for global productivity gradients. *Geology*, *34*(4), 233–236. https://doi.org/10.1130/G22381.1

Gillooly, J. F., Brown, J. H., West, G. B., Savage, V. M., & Charnov, E. L. (2001). Effects on size and temperature on metabolic rate. *Science*, *293*, 2248–2251. https://doi.org/10.1126/science.1061967

Giusberti, L., Coccioni, R., Sprovieri, M., & Tateo, F. (2009). Perturbation at the sea floor during the Paleocene-Eocene thermal maximum: Evidence from benthic foraminifera at Contessa road, Italy. *Marine Micropaleontology*, *70*, 102–119. https://doi.org/10.1016/j.marmicro.2008.11.003

Gooday, A. J. (2003). Benthic foraminifera (Protista) as tools in deep-water paleoceanography: Environmental influences on faunal characteristics. *Advances in Marine Biology*, *46*, 1–90. https://doi.org/10.1016/s0065-2881(03)46002-1

Hague, A. M., Thomas, D. J., Huber, M., Korty, R., Woodard, S. C., & Jones, L. B. (2012). Convection of North Pacific deep water during the early Cenozoic. *Geology*, *40*(6), 527–530. https://doi.org/10.1130/g32886.1

Hammer, Ø., Harper, D. A. T., & Ryan, P. D. (2001). PAST: Paleontological statistics software package for education and data analysis. *Palaeontologia Electronica*, *4*(1), 1–9.

Haq, B. U., & Lohmann, G. P. (1976). Early Cenozoic calcareous nannoplankton biogeography of the Atlantic Ocean. *Marine Micropaleontology*, *1*, 119–194. https://doi.org/10.1016/0377-8398(76)90008-6

Hayward, B. W., Kawagata, S., Sabaa, A. T., Grenfell, H. R., van Kerckhoven, L., Johnson, K., & Thomas, E. (2012). *The last global extinction (Mid-Pleistocene) of deep-sea benthic foraminifera (Chrysalogoniidae, Ellipsoidinidae, Glandulonodosariidae, Plectofrondicularиidae, Pleurostomellidae, Stilostomellidae), their Late Cretaceous-Cenozoic history and taxonomy*. (Vol. 43, p. 408). Cushman Foundation for Foraminiferal Research Special Publication.

Herguera, J. C., & Berger, W. (1991). Paleoproductivity from benthonic foraminifera abundance: Glacial to postglacial change in the west-equatorial Pacific. *Geology*, *19*, 1173–1176. https://doi.org/10.1130/0091-7613(1991)019<1173:pfbfag>2.3.co;2

Hines, B., Hollis, C., Atkins, C., Baker, J., Morgans, H., & Strong, C. (2017). Reduction of oceanic temperature gradients in the early Eocene Southwest Pacific Ocean. *Palaeogeography, Palaeoclimatology, Palaeoecology*, *475*, 41–54. https://doi.org/10.1016/j.palaeo.2017.02.037

Hoegh-Guldberg, O., & Bruno, J. F. (2010). The impact of climate change on the world's marine ecosystems. *Science*, *328*(5985), 1523–1528. https://doi.org/10.1126/science.1189930

Hollis, C. J., Dickens, G. R., Field, B. D., Jones, C. J., & Strong, C. P. (2005). The Paleocene-Eocene transition at Mead Stream, New Zealand: A southern Pacific record of early Cenozoic global change. *Palaeogeography, Palaeoclimatology, Palaeoecology*, *215*, 313–343. https://doi.org/10.1016/j.palaeo.2004.09.011

Hollis, C. J., Dunkley Jones, T., Anagnostou, E., Bijl, P. K., Cramwinckel, M. J., Cui, Y., et al. (2019). The DeepMIP contribution to PMIP4: Methodologies for selection, compilation and analysis of latest Paleocene and early Eocene climate proxy data, incorporating version 0.1 of the DeepMIP database. *Geoscientific Model Development*, *12*(7), 3149–3206. https://doi.org/10.5194/gmd-2018-309

Hollis, C. J., Handley, L., Crouch, E. M., Morgans, H. E. G., Baker, J. A., Creech, J., et al. (2009). Tropical sea temperatures in the high-latitude South Pacific. *Geology*, *37*, 99–102. https://doi.org/10.1130/g25200a.1

Hollis, C. J., Taylor, K. W., Handley, L., Pancost, R. D., Huber, M., Creech, J. B., et al. (2012). Early Paleogene temperature history of the Southwest Pacific Ocean: Reconciling proxies and models. *Earth and Planetary Science Letters*, *349*, 53–66. https://doi.org/10.1016/j.epsl.2012.06.024

Hottinger, L. C. (2000). Functional morphology of benthic foraminiferal shells, envelopes of cells beyond measure. *Micropaleontology*, *46*(1), 57–86.

Hottinger, L. C. (2006). The "face" of benthic foraminifera. *Bollettino-Societa Paleontologica Italiana*, *45*, 75–89.

Huber, M., Brinkhuis, H., Stickley, C. E., Döös, K., Sluijs, A., Warnaar, J., et al. (2004). Eocene circulation of the Southern Ocean: Was Antarctica kept warm by subtropical waters? *Paleoceanography*, *19*, PA4026. https://doi.org/10.1029/PA001022

Huber, M., & Nof, D. (2006). The ocean circulation in the southern hemisphere and its climatic impacts in the Eocene. *Palaeogeography, Palaeoclimatology, Palaeoecology*, *231*, 9–28. https://doi.org/10.1016/j.palaeo.2005.07.037

Printed by [Icelandair ehf - 185.056.012.142 - /doi/epdf/10.1029/2020PA004179] at [04/08/2021].

Huck, C. E., van de Flierdt, T., Boharty, S. M., & Hammond, S. J. (2017). Antarctic climate, Southern Ocean circulation patterns, and deep water formation during the Eocene. *Palaeoceanography*, *32*, 674–691. https://doi.org/10.1002/2017pa003135

Inglis, G. N., Bragg, F., Burls, N. J., Cramwinckel, M. J., Evans, D., Foster, G. L., et al. (2020). Global mean surface temperature and climate sensitivity of the early Eocene climatic optimum (EECO), Paleocene-Eocene Thermal Maximum (PETM), and latest Paleocene. *Climate of the Past*, *16*(5), 1953–1968. https://doi.org/10.5194/cp-16-1953-2020

Inglis, G. N., Farnsworth, A., Lunt, D., Foster, G. L., Hollis, C. J., Pagani, M., et al. (2015). Descent toward the Icehouse: Eocene sea surface cooling inferred from GDGT distributions. *Paleoceanography*, *29*, 1000–1020. https://doi.org/10.1002/2014PA002723

Jennions, S. M., Thomas, E., Schmidt, D. N., Lunt, D., & Ridgwell, A. (2015). Changes in benthic ecosystems and ocean circulation in the Southeast Atlantic across Eocene thermal maximum 2. *Paleoceanography*, *30*, 1059–1077. https://doi.org/10.1002/2015PA002821

John, E. H., Pearson, P. N., Coxall, H. K., Birch, H., Wade, B. S., & Foster, G. L. (2013). Warm ocean processes and carbon cycling in the Eocene. *Philosophical Transactions of the Royal Society A: Mathematical, Physical and Engineering Sciences*, *371*, 20130099. https://doi.org/10.1098/rsta.2013.0099

John, E. H., Wilson, J. D., Pearson, P. N., & Ridgwell, A. (2014). Temperature-dependent remineralization and carbon cycling in the warm Eocene oceans. *Palaeogeography, Palaeoclimatology, Palaeoecology*, *413*, 158–166. https://doi.org/10.1016/j.palaeo.2014.05.019

Jorissen, F. J., Fontanier, C., & Thomas, E. (2007). Paleoceanographical proxies based on deep-sea benthic foraminiferal assemblage characteristics. In C. Hillaire-Marcel, & A. de Vernal (Eds.), *Proxies in late Cenozoic paleoceanography (Pt. 2). Biological tracers and biomarkers* (pp. 263–325). Elsevier. https://doi.org/10.1016/s1572-5480(07)01012-3

Katz, M. E., Katz, D. R., Wright, J. D., Miller, K. G., Pak, D. K., Shackleton, N. J., & Thomas, E. (2003). Early Cenozoic benthic foraminiferal isotopes: Species reliability and interspecies correction factors. *Paleoceanography*, *18*, 1024. https://doi.org/10.1029/2002PA000798

Kawahata, H., Nomura, R., Matsumoto, K., & Nishi, H. (2015). Linkage of deep sea rapid acidification process and extinction of benthic foraminifera in the deep sea at the Paleocene/Eocene transition. *Island Arc*, *24*, 301–316. https://doi.org/10.1111/iar.12106

Kelly, D. C., Zachos, J. C., Bralower, T. J., & Schellenberg, S. A. (2005). Enhanced terrestrial weathering/runoff and surface ocean carbonate production during the recovery stages of the Paleocene-Eocene thermal maximum. *Paleoceanography*, *20*(4), PA4023. https://doi.org/10.1029/2005pa001163

Kirtland Turner, S., Sexton, P. F., Charles, C. D., & Norris, R. D. (2014). Persistence of carbón release events through the peak of early Eocene global warmth. *Nature Geoscience*, *7*, 748–751. https://doi.org/10.1038/ngeo2240

Lauretano, V., Littler, K., Polling, M., Zachos, J. C., & Lourens, L. J. (2015). Frequency, magnitude and character of hyperthermal events at the onset of the early Eocene climatic optimum. *Climate of the Past*, *11*(10), 1313–1324. https://doi.org/10.5194/cp-11-1313-2015

Littler, K., Röhl, U., Westerhold, T., & Zachos, J. C. (2014). A high-resolution benthic stable-isotope record for the South Atlantic: Implications for orbital-scale changes in Late Paleocene–Early Eocene climate and carbon cycling. *Earth and Planetary Science Letters*, *401*, 18–30. https://doi.org/10.1016/j.epsl.2014.05.054

Lourens, L., Sluijs, A., Kroon, D., Zachos, J. C., Thomas, E., Roehl, U., et al. (2005). Astronomical modulation of late Palaeocene to early Eocene global warming events. *Nature*, *435*, 1083–1087. https://doi.org/10.1038/nature038110.1038/nature03814

Luciani, V., Dickens, G., Backman, J., Fornaciari, E., Giusberti, L., Agnini, C., & D'Onofrio, R. (2016). Major perturbations in the global carbon cycle and photosymbiont-bearing planktic foraminifera during the early Eocene. *Climate of the Past*, *12*(4), 981–1007. https://doi.org/10.5194/cp-12-981-2016

Luciani, V., D'Onofrio, R., Dickens, G., & Wade, B. S. (2017). Did photosymbiont bleaching lead to the demise of planktic foraminifer *Morozovella* at the early Eocene climatic optimum? *Paleoceanography*, *32*, 1115–1136. https://doi.org/10.1002/2017PA003138

Lunt, D. J., Ridgwell, A., Sluijs, A., Zachos, J., Hunter, S., & Haywood, A. (2011). A model for orbital pacing of methane hydrate destabilization during the Palaeogene. *Nature Geoscience*, *4*(11), 775–778. https://doi.org/10.1038/ngeo1266

Ma, Z., Gray, E., Thomas, E., Murphy, B., Zachos, J. C., & Paytan, A. (2014). Carbon sequestration during the Paleocene-Eocene thermal maximum by an efficient biological pump. *Nature Geoscience*, *7*, 382–388. https://doi.org/10.1038/NGEO2139

Mancin, N., Hayward, B. W., Trattenero, I., Cobianchi, M., & Lupi, C. (2013). Can the morphology of deep-sea benthic foraminifera reveal what caused their extinction during the mid-Pleistocene climate transition? *Marine Micropaleontology*, *104*, 53–70. https://doi.org/10.1016/j.marmicro.2013.09.004

Martini, E. (1971). Standard Tertiary and Quaternary calcareous nannoplankton zonation. In A. Farinacci (Ed.), *Proceedings 2nd International Conference Planktonic Microfossils Roma* (pp. 739–785). Tecnoscienza.

Matthews, K. J., Maloney, K. T., Zahirovic, S., Williams, S. E., Seton, M., & Müller, R. D. (2016). Global plate boundary evolution and kinematics since the late Paleozoic. *Global and Planetary Change*, *146*, 226–250. https://doi.org/10.1016/j.gloplacha.2016.10.002

Monechi, S., Buccianti, A., & Gardin, S. (2000). Biotic signals from nannoflora across the iridium anomaly in the upper Eocene of the Massignano section: Evidence from statistical analysis. *Marine Micropaleontology*, *39*, 219–237. https://doi.org/10.1016/S0377-8398(00)00022-0

Monechi, S., & Thierstein, H. R. (1985). Late Cretaceous-Eocene nannofossil and magnetostratigraphic correlations near Gubbio, Italy. *Marine Micropaleontology*, *9*(5), 419–440. https://doi.org/10.1016/0377-8398(85)90009-X

Murray, J. W. (2006). *Ecology and applications of benthic foraminifera* (p. 426). Cambridge University Press.

Newsam, C., Bown, P. R., Wade, B. S., & Jones, H. L. (2017). Muted calcareous nannoplankton response at the middle/late Eocene Turnover event in the western North Atlantic Ocean. *Newsletters on Stratigraphy*, *50*, 297–309. https://doi.org/10.1127/nos/2016/0306

Nguyen, T. M. P., Petrizzo, M. R., & Speijer, R. P. (2009). Experimental dissolution of a fossil foraminiferal assemblage (Paleocene-Eocene thermal maximum, Dababiya, Egypt): Implications for paleoenvironmental reconstructions. *Marine Micropaleontology*, *73*(3–4), 241–258. https://doi.org/10.1016/j.marmicro.2009.10.005

Nomura, R. (1995). Paleogene to Neogene deep-sea paleoceanography in the Eastern Indian Ocean: Benthic foraminifera from ODP Sites 747, 757 and 758. *Micropaleontology*, *41*, 251–290. https://doi.org/10.2307/1485862

Okada, H., & Bukry, D. (1980). Supplementary modification and introduction of code numbers to the low-latitude coccolith biostratigraphic zonation (Bukry, 1973; 1975). *Marine Micropaleontology*, *5*, 321–325. https://doi.org/10.1016/0377-8398(80)90

Ortiz, S., Alegret, L., Payros, A., Orue-Etxebarria, X., Apellaniz, E., & Molina, E. (2011). Distribution patterns of benthic foraminifera across the Ypresian-Lutetian Gorrondatxe section, northern Spain: Response to sedimentary disturbance. *Marine Micropaleontology*, *78*, 1–13. https://doi.org/10.1016/j.marmicro.2010.09.004

Pearson, P. N., & Palmer, M. R. (2000). Atmospheric carbon dioxide concentrations over the past 60 million years. *Nature*, *406*, 695–699. https://doi.org/10.1038/35021000

Penman, D. E. (2016). Silicate weathering and North Atlantic silica burial during the Paleocene-Eocene thermal maximum. *Geology*, *44*(9), 731–734. https://doi.org/10.1130/g37704.1

Penman, D. E., Keller, A., D'haenens, S., Kirtland Turner, S., & Hull, P. M. (2019). Atlantic deep-sea cherts associated with Eocene hyperthermal events. *Paleoceanography and Paleoclimatology*, *34*, 287–299. https://doi.org/10.1029/2018PA003503

Printed by [Icelandair ehf - 185.056.012.142 - /doi/epdf/10.1029/2020PA004179] at [04/08/2021].

Perch-Nielsen, K. (1985). Cenozoic calcareous nannofossils. In H. M. Bolli, J. B. Saunders, & K. Perch-Nielsen (Eds.), *Plankton stratigraphy* (pp. 427–554). Cambridge University Press

Persico, D., & Villa, G. (2004). Eocene-Oligocene calcareous nannofossils from Maud rise and Kerguelen Plateau (Antarctica): Paleoecological and paleoceanographic implications. *Marine Micropaleontology*, *52*, 153–179. https://doi.org/10.1016/j.marmicro.2004.05.002

Rivero-Cuesta, L., Westerhold, T., Dallanave, E., Agnini, C., Alegret, L., & Alegret, L. (2019). Paleoenvironmental changes at ODP Site 702 (South Atlantic): Anatomy of the middle Eocene climatic optimum. *Paleoceanography and Paleoclimatology*, *34*(12), 2047–2066. https://doi.org/10.1029/2019PA003806

Röhl, U., Westerhold, T., Monechi, S., Thomas, E., & Zachos, J. C. (2005). The third and final early Eocene thermal maximum: Characteristics, timing, and mechanisms of the "X" event. *Geological Society of America*, *37*, 264.

Royer, D. L., Berner, R. A., & Park, J. (2007). Climate sensitivity constrained by CO_2 concentrations over the past 420 million years. *Nature*, *446*, 530–532. https://doi.org/10.1038/nature05699

Schmiedl, G., Pfeilsticker, M., Hemleben, C., & Mackensen, A. (2004). Environmental and biological effects on the stable isotope composition of recent deep-sea benthic foraminifera from the western Mediterranean Sea. *Marine Micropaleontology*, *51*(1–2), 129–152. https://doi.org/10.1016/j.marmicro.2003.10.001

Schneider, L. J., Bralower, T. J., & Kump, L. R. (2011). Response of nannoplankton to early Eocene ocean destratification. *Palaeogeography, Palaeoclimatology, Palaeoecology*, *310*, 152–162. https://doi.org/10.1016/j.palaeo.2011.06.018

Sen Gupta, B. K. (1999). Introduction to modern Foraminifera. In B. K. Sen Gupta (Ed.), *Systematics of modern foraminifera* (pp. 7–36). Kluwer Academic Publishers. https://doi.org/10.1007/0-306-48104-9_2

Sen Gupta, B. K., & Machain-Castillo, M. L. (1993). Benthic foraminifera in oxygen-poor habitats. *Marine Micropaleontology*, *20*, 183–201. https://doi.org/10.1016/0377-8398(93)90032-s

Shackleton, N. J., & Kennett, J. P. (1975). Paleotemperature history of the Cenozoic and the initiation of Antarctic glaciation: Oxygen and carbon isotope analyses in DSDP Sites 277, 279, and 281. In J. P. Kennett, & R. E. Houtz (Eds.), *Initial reports of the deep sea drilling project* (Vol. 29, pp. 743–755). U.S. Governmen Printing Office.

Shipboard Scientific Party. (1973a). Site 206. With contributions by D. Burns and P. N. Webb. In R. E. Burns, & J. E. Andrews (Eds.), *Initial reports of the deep sea drilling project* (Vol. 21, pp. 103–195). U.S. Government Printing Office. https://doi.org/10.2973/dsdp.proc.21.106.1973

Shipboard Scientific Party. (1973b). Site 207. With contributions by D. Burns, W. A. Watters, and P. N. Webb. In R. E. Burns, & J. E. Andrews, (Eds.), *Initial reports of the deep sea drilling project* (Vol. 21, pp. 197–269). U.S. Government Printing Office. https://doi.org/10.2973/dsdp.proc.21.107.1973

Shipboard Scientific Party. (1973c). Site 210. In R. E. Burns, & J. E. Andrews, (Eds.), *Initial reports of the deep sea drilling project* (Vol. 21, pp. 369–440). U.S. Government Printing Office. https://doi.org/10.2973/dsdp.proc.21.110.1973

Shipboard Scientific Party. (1975). Site 277. In J. P. Kennett, & R. E. Houtz, (Eds.), *Initial reports of the deep sea drilling project* (Vol. 29, pp. 45–120). U.S. Government Printing Office. https://doi.org/10.2973/dsdp.proc.29.104.1975

Sijp, W. P., Von Der Heydt, A. S., & Bijl, P. K. (2016). Model simulations of early westward flow across the Tasman Gateway during the early Eocene. *Climate of the Past*, *12*, 807–817. https://doi.org/10.5194/cp-12-807-2016

Slotnick, B. S., Dickens, G. R., Hollis, C. J., Crampton, J. S., Strong, C. P., & Phillips, A. (2015). The onset of the early Eocene climatic optimum at branch stream, Clarence River valley, New Zealand. *New Zealand Journal of Geology and Geophysics*, *58*, 262–280. https://doi.org/10.1080/00288306.2015.1063514

Slotnick, B. S., Dickens, G. R., Nicolo, M. J., Hollis, C. J., Crampton, J. S., Zachos, J. C., & Sluijs, A. (2012). Large-amplitude variations in carbon cycling and terretrial weathering during the latest Paleocene and earliest Eocene: The record at Mead Stream, New Zealand. *The Journal of Geology*, *120*, 487–505. https://doi.org/10.1086/666743

Speijer, R. P., Scheibner, C., Stassen, P., & Morsi, A.-M. (2012). Response of marine ecosystems to deep-time global warming: A synthesis of biotic patterns across the Paleocene-Eocene thermal maximum (PETM). *Austrian Journal of Earth Sciences*, *105*, 6–16.

Steineck, P. L., & Thomas, E. (1996). The latest Paleocene crisis in the deep sea: Ostracode succession at Maud rise, Southern Ocean. *Geology*, *24*, 583–586. https://doi.org/10.1130/0091-7613(1996)024<0583:tlpcit>2.3.co;2

Sutherland, R., Dickens, G. R., Blum, P., Agnini, C., Alegret, L., Asatryan, G., et al. (2019). *Tasman frontier subduction initiation and paleogene climate* (Vol. 371). International Ocean Discovery Program.

Sutherland, R., Dickens, G. R., Blum, P., Agnini, C., Alegret, L., Asatryan, G., et al. (2020). Continental-scale geographic change across Zealandia during Paleogene subduction initiation. *Geology*, *48*, 419–424. https://doi.org/10.1130/G47008.1

Sutherland, R., Dickens, G. R., Blum, P., Agnini, C., Alegret, L., Bhattacharya, J., et al. (2019). Site U1510. In R. Sutherland, G. R. Dickens, & P. Blum (Eds.), *The expedition 371 Scientists, tasman frontier subduction initiation and Paleogene climate* (Vol. 371). International Ocean Discovery Program. https://doi.org/10.14379/iodp.proc.371.107.2019

Sutherland, R., Dickens, G. R., Blum, P., & the Expedition 371 Scientists. (2018). *Expedition 371 Preliminary Report: Tasman frontier subduction initiation and paleogene climate*. International Ocean Discovery Program. https://doi.org/10.14379/iodp.pr.371.2018

Takeda, K., & Kaiho, K. (2007). Faunal turnovers in central Pacific benthic foraminifera during the Paleocene-Eocene thermal maximum. *Palaeogeography, Palaeoclimatology, Palaeoecology*, *251*, 175–197. https://doi.org/10.1016/j.palaeo.2007.02.026

Thomas, D. J. (2004). Evidence for deep-water production in the North Pacific Ocean during the early Cenozoic warm interval. *Nature*, *430*, 65–68. https://doi.org/10.1038/nature02639

Thomas, D. J., Lyle, M., Moore, T. C., Jr, & Rea, D. K. (2008). Paleogene deepwater mass composition of the tropical Pacific and implications for the thermohaline circulation in a greenhouse world. *Geochemistry, Geophysics, Geosystems*, *9*, Q02002. https://doi.org/10.1029/2007GC001748

Thomas, E. (2003). Extinction and food at the seafloor: A high-resolution benthic foraminiferal record across the initial Eocene thermal maximum, southern ocean Site 690. In S. L. Wing, P. D. Gingerich, B. Schmitz, & E. Thomas (Eds.), *Causes and consequences of globally warm climates in the early Paleogene* (pp. 319–332). Geological Society of America Special Paper 369. https://doi.org/10.1130/0-8137-2369-8.319

Thomas, E. (2007). Cenozoic mass extinctions in the deep sea: What perturbs the largest habitat on Earth? In S. Monechi, R. Coccioni, & M. R. Rampino (Eds.), *Large ecosystem perturbations: Causes and consequences* (Vol. 424, pp. 1–23). Geological Society of America Special Papers.

Thomas, E., Boscolo-Galazzo, F., Balestra, B., Monechi, S., Donner, B., & Röhl, U. (2018). Early Eocene thermal maximum 3: Biotic response at Walvis Ridge (SE Atlantic Ocean). *Paleoceanography and Paleoclimatology*, *33*, 862–883. https://doi.org/10.1029/2018PA003375

Thomas, E., Zachos, J. C., & Bralower, T. J. (2000). Deep-sea environments on a warm Earth: Latest Paleocene-early Eocene. In B. Huber, K. MacLeod, & S. Wing (Eds.), *Warm climates in Earth history* (pp. 132–160). Cambridge University Press.

Printed by [Icelandair ehf - 185.056.012.142 - /doi/epdf/10.1029/2020PA004179] at [04/08/2021].

Torsvik, T. H., Van der Voo, R., Preeden, U., Mac Niocaill, C., Steinberger, B., Doubrovine, P. V., et al. (2012). Phanerozoic polar wander, palaeogeography and dynamics. *Earth-Science Reviews*, *114*(3), 325–368. https://doi.org/10.1016/j.earscirev.2012.06.007

Villa, G., Fioroni, C., Pea, L., Bohaty, S. M., & Persico, D. (2008). Middle Eocene-late Oligocene climate variability: Calcareous nannofossil response at Kerguelen Plateau, Site 748. *Marine Micropaleontology*, *69*, 173–192. https://doi.org/10.1016/j.marmicro.2008.07.00

Villa, G., Fioroni, C., Persico, D., Roberts, A. P., & Florindo, F. (2014). Middle Eocene to late Oligocene Antarctic glaciation/deglaciation and Southern Ocean productivity. *Paleoceanography*, *29*, 223–237. https://doi.org/10.1002/2013PA002518

Wei, W., & Wise, S. W., Jr. (1990). Biogeographic gradients of middle Eocene-Oligocene calcareous nannoplankton in the South Atlantic Ocean. *Palaeogeography, Palaeoclimatology, Palaeoecology*, *79*, 29–61. https://doi.org/10.1016/0031-0182(90)90104-F

Westerhold, T., Marwan, N., Drury, A. J., Liebrand, D., Agnini, C., Anagnostou, E., et al. (2020). An astronomically dated record of Earth's climate and its predictability over the last 66 million years. *Science*, *369*, 1383–1387. https://doi.org/10.1126/science.aba6853

Westerhold, T., & Röhl, U. (2009). High resolution cyclostratigraphy of the early Eocene—New insights into the origin of the Cenozoic cooling trend. *Climate of the Past*, *5*, 309–327. https://doi.org/10.5194/cp-5-309-2009/

Westerhold, T., Röhl, U., Donner, B., & Zachos, J. C. (2018). Global extent of early Eocene hyperthermal events: A new Pacific benthic foraminiferal isotope record from Shatsky Rise (ODP Site 1209). *Paleoceanography and Paleoclimatology*, *33*, 626–642. https://doi.org/10.1029/2017PA003306

Westerhold, T., Röhl, U., Frederichs, T., Agnini, C., Raffi, I., Zachos, J. C., & Wilkens, R. H. (2017). Astronomical calibration of the Ypresian time scale: Implications for seafloor spreading rates and the chaotic behaviour of the solar system? *Climate of the PastClimate of the Past*, *13*, 1–24. https://doi.org/10.5194/cp-2017-15

Witkowski, J., Penman, D. E., Bryłka, K., Wade, B. S., Matting, S., Harwood, D. M., & Bohaty, S. M. (2020). Early Paleogene biosiliceous sedimentation in the Atlantic Ocean: Testing the inorganic origin hypothesis for Paleocene and Eocene chert and porcellanite. *Palaeogeography, Palaeoclimatology, Palaeoecology*, *556*, 109896. https://doi.org/10.1016/j.palaeo.2020.109896

Zachos, J. C., Dickens, G. R., & Zeebe, R. E. (2008). An early Cenozoic perspective on greenhouse warming and carbon-cycle dynamics. *Nature*, *451*, 279–283. https://doi.org/10.1038/nature06588

Zeebe, R., & Lourens, L. (2019). Solar System chaos and the Paleocene-Eocene boundary age constrained by geology and astronomy. *Science*, *365*(6456), 4. https://doi.org/10.1126/science.aax0612

Printed by [Icelandair ehf - 185.056.012.142 - /doi/epdf/10.1029/2020PA004179] at [04/08/2021].